

Clausius–Clapeyron Scaling of CAPE from Analytical Solutions to RCE

DAVID M. ROMPS

Department of Earth and Planetary Science, University of California, Berkeley, and Climate and Ecosystem Sciences Division, Lawrence Berkeley National Laboratory, Berkeley, California

(Manuscript received 30 October 2015, in final form 5 June 2016)

ABSTRACT

By deriving analytical solutions to radiative–convective equilibrium (RCE), it is shown mathematically that convective available potential energy (CAPE) exhibits Clausius–Clapeyron (CC) scaling over a wide range of surface temperatures up to 310 K. Above 310 K, CAPE deviates from CC scaling and even decreases with warming at very high surface temperatures. At the surface temperature of the current tropics, the analytical solutions predict that CAPE increases at a rate of about 6%–7% per kelvin of surface warming. The analytical solutions also provide insight on how the tropopause height and stratospheric humidity change with warming. Changes in the tropopause height exhibit CC scaling, with the tropopause rising by about 400 m per kelvin of surface warming at current tropical temperatures and by about 1–2 km K^{−1} at surface temperatures in the range of 320–340 K. The specific humidity of the stratosphere exhibits super-CC scaling at temperatures moderately warmer than the current tropics. With a surface temperature of the current tropics, the stratospheric specific humidity increases by about 6% per kelvin of surface warming, but the rate of increase is as high as 30% K^{−1} at warmer surface temperatures.

1. Introduction

Convective available potential energy (CAPE), which is a function of the atmosphere's temperature profile and near-surface humidity, is the maximum specific vertical kinetic energy $w^2/2$ that storm clouds can theoretically attain while rising. CAPE plays a critical role in the prediction of severe weather (Johns and Doswell III 1992; Brooks et al. 1994; Rasmussen and Blanchard 1998; Rasmussen 2003; Brooks et al. 2003) and lightning (Williams et al. 1992, 2002; Pawar et al. 2012; Murugavel et al. 2014; Romps et al. 2014). Of particular importance, therefore, is the question of how CAPE will change with global warming.

Global climate models predict robust increases in midlatitude CAPE and associated increases in the occurrence of severe weather (Trapp et al. 2007, 2009; Diffenbaugh et al. 2013; Seeley and Romps 2015a) and the frequency of lightning strikes (Romps et al. 2014). In the tropics, global climate models predict an increase in CAPE with surface temperature on the order of 10% K^{−1} (Sobel and Camargo 2011) and cloud-resolving

simulations report similar sensitivities: 8% (Romps 2011)¹, 8% (Muller et al. 2011), 12% (Singh and O'Gorman 2013, hereafter SO13), and 7% K^{−1} (Seeley and Romps 2015b).

This strong sensitivity of CAPE to temperature is reminiscent of the Clausius–Clapeyron (CC) scaling of specific humidity, which, at constant relative humidity, increases at 6%–7% K^{−1} in the lower tropical troposphere. But what is the connection, if any, between the Clausius–Clapeyron scaling of water vapor and the rapid increase in CAPE? A common hand-waving argument goes like this: the condensation of water vapor allows clouds to maintain their buoyancy as they rise, so a fractional increase in available water vapor should lead to the same fractional increase in buoyancy and, therefore, CAPE. This argument is wholly unsatisfactory because it is devoid of physics and is in no way obviously true. For this argument to be satisfactory, we would need to imagine an atmosphere with a dry adiabatic lapse rate. In this imaginary world, an increase of 6%–7% K^{−1}

Corresponding author address: David M. Romps, 307 McCone Hall, University of California, Berkeley, Berkeley, CA 94720.
E-mail: romps@berkeley.edu

¹In Romps (2011), the sensitivity of CAPE was incorrectly reported as 6%–7% per doubling of CO₂. The correct number, as obtained from Fig. 1 of Romps (2011) and from the original data files, is 8% K^{−1}.

in near-surface water vapor would obviously lead to a comparable increase in the buoyancy of moist adiabatic clouds in the middle and upper troposphere. Of course, we do not live in such a world. Therefore, if we are to make any real progress on understanding whether CAPE exhibits Clausius–Clapeyron scaling, we must first develop a comprehensive theory for CAPE.

Over the past 20 yr, three different theories have been advanced for CAPE: a theory based on the entropy budget (Rennó and Ingersoll 1996; Emanuel and Bister 1996), a theory based on the two scale heights of water (Mapes 2001), and a theory based on zero-buoyancy convection (SO13). We will briefly review these here. We will see how the first was disproved, why the second faces substantial difficulties, and why the third is most likely correct.

The first theory for CAPE was proposed simultaneously by Rennó and Ingersoll (1996) and Emanuel and Bister (1996). In this theory, the convecting atmosphere is viewed as a heat engine with heat added at the surface temperature T_s , heat removed at the colder radiative temperature T_r , and clouds performing work in the process of moving heat from T_s to T_r . By constructing a simple entropy budget, we arrive at

$$M\text{CAPE} \approx \eta Q, \quad (1)$$

where M is the convective mass flux, Q is the net radiative cooling of the atmosphere, and $\eta = 1 - T_r/T_s$ is the Carnot efficiency. By prescribing an updraft area fraction and relating M to the speed given by $\sqrt{2\text{CAPE}}$, this can be recast as an explicit expression for CAPE. Unfortunately, several problems render this theory untenable. For one, the theory ignores the large entropy source due to the diffusion of water vapor (Pauluis and Held 2002a) or, equivalently, the fact that condensational heating occurs at a significantly colder temperature than the surface (Romps 2008). Also, clouds must compete for the entropically available work with the frictional dissipation of falling condensates (Pauluis et al. 2000) or, when the entropy budget is written in another form, with the work required to lift both condensates and water vapor (Romps 2008). Furthermore, clouds are highly entraining (Kuang and Bretherton 2006; Fierro et al. 2009; Romps and Kuang 2010), so they do not attain the buoyancies predicted by the undiluted ascent used to calculate CAPE.

The second theory, proposed by Mapes (2001), postulates that CAPE is present because of the mismatch between the profile of latent heating of an adiabatic parcel (which heats at a mean height of H_l) and the profile of radiative cooling (which cools at a mean height

of H_r). According to this theory, the mismatch between H_l and H_r must be made up by positive sensible fluxes from H_l to H_r . Positive sensible fluxes are accomplished by having updrafts that are warmer and, therefore, more buoyant than the environment. Assuming that clouds are nonentraining, CAPE is then equal to the vertical integral of cloud buoyancy. As shown in appendix A, we can then relate cloud buoyancy to the sensible heat fluxes and then use the energy budget to obtain

$$M\text{CAPE} \approx \eta' Q, \quad (2)$$

where $\eta' = g(H_r - H_l)/c_p T_0$ and T_0 is a typical tropospheric temperature. While there is no doubt that the energy budget of the troposphere must be closed and that sensible heat fluxes play an important role, there are several reasons to doubt Eq. (2) and, for that matter, to doubt that the energy budget places a significant constraint on CAPE at all. First, as noted above, most convecting clouds are highly entraining, so their buoyancy b does not equal the buoyancy of the nonentraining parcel used to calculate CAPE. Clouds that are either nonentraining or nearly nonentraining are likely too infrequent to be dominant players in the atmospheric energy budget, and this suggests that CAPE is unlikely to be constrained by the energy budget. Second, the energy budget of the atmosphere is much more complicated than simply radiation, condensation in non-entraining parcels, and sensible fluxes. Evaporation of condensates is a dominant term in the energy budget. With typical precipitation efficiencies around 25% (Pauluis and Held 2002b; Romps 2011), the gross condensational heating C and the gross evaporative cooling E are related to each other by $(C - E)/C = 25\%$, and the net radiative cooling Q is related to them both by $Q = C - E$. Solving for E in terms of Q , we find that $E = 3Q$, so the evaporative cooling is 3 times larger than the radiative cooling. The vertical structure of gross cooling (radiative plus evaporative) is, therefore, dominated by evaporation, and any theory for CAPE that relies on the vertical structure of radiative cooling alone is, at best, incomplete. Third, a theory for CAPE that is based on the need to move sensible heat from a warm place to a cold place will be closely related to the heat-engine perspective of the atmosphere, which can be described by the entropy budget. The entropy budget, however, does not appear to be a promising starting point for developing a theory of CAPE, since the dissipation of kinetic energy (produced by the work of buoyant ascent) is two orders of magnitude smaller than the dominant terms in the entropy budget (Pauluis and Held 2002b; Romps 2008).

The third theory advanced by SO13 dispenses with the heat-engine perspective altogether. This theory begins with the observation that most convecting clouds are highly entraining and, therefore, have buoyancies that are a small fraction of the buoyancy of a theoretical nonentraining parcel. To illustrate this fact, note that a typical value of CAPE in the deeply convecting tropics is 3000 J kg^{-1} (e.g., Williams and Renno 1993). Approximating CAPE as $Hg\Delta T/T$, where $H \approx 10^4 \text{ m}$ is the depth of the troposphere, $g \approx 10 \text{ m s}^{-2}$, and $T \approx 300 \text{ K}$, we find that the temperature excess of a lifted undiluted parcel is $\Delta T \approx 10 \text{ K}$. On the other hand, the typical buoyancy of tropical deep convection is in the range of 0.3–0.5 K [see Fig. 2 of Romps and Öktem (2015)]. The smallness of typical cloud buoyancies relative to the buoyancies of undiluted parcels suggests that CAPE can be understood by approximating typical cloud buoyancies as zero. Note that, with zero buoyancy, these clouds can do no work, so there is no room for a heat engine in this theory.

The zero-buoyancy approximation allows CAPE to be calculated numerically for radiative–convective equilibrium (RCE) so long as the relative humidity and the level of neutral buoyancy are specified. As shown by SO13, the zero-buoyancy approximation can be used to predict profiles of nonentraining-parcel buoyancy and values of CAPE that are strikingly similar to those diagnosed from cloud-resolving simulations of RCE. This theory was further validated by Seeley and Romps (2015b), who showed that the zero-buoyancy approximation accurately predicts the changes in CAPE caused by both variations in relative humidity and in surface temperature.

Building on the initial success of SO13, Romps (2014a, hereafter abbreviated as R14) combined the zero-buoyancy approximation with the bulk-plume equations, which approximate updrafts and the environment as homogeneous at each height. Whereas the theory of SO13 must be fed the profile of relative humidity as an input, the theory of R14 predicts the RCE profiles of both temperature and relative humidity. In particular, this theory makes predictions for how the profile of relative humidity changes with warming, and these predictions were validated by R14 against cloud-resolving simulations.

As in the work of SO13, the theory of R14 comprises a set of equations that must be integrated upward in height numerically. While not difficult to integrate, the fact that the solutions are numerical, rather than analytical, makes it difficult to glean insights from them. In this paper, analytical solutions are sought to the equations of R14. Section 2 presents these solutions, which include an analytical expression for CAPE in RCE.

Section 3 explores some of the implications of these solutions for the height of the tropopause, the specific humidity of the tropical stratosphere, and, of course, the scaling of CAPE with temperature.

2. Theory

This section presents analytical solutions for the thermodynamic structure of radiative–convective equilibrium. The derivations, which are given in appendix B, build on the work of R14. In short, R14 uses the zero-buoyancy bulk-plume equations to derive expressions for relative humidity and the lapse rate. As in R14, we assume that the convective mass flux M and precipitation efficiency (PE) are all constant throughout the troposphere. Here, $\text{PE}(z)$ is defined to be the ratio of net condensation to gross condensation at height z . In a departure from R14, we assume that the relative humidity (RH) is constant throughout the troposphere. This assumption is made to simplify the problem and to make it analytically soluble, but it is not imposed by introducing artificial sources and sinks of water. Instead, we require that the relative humidity, precipitation efficiency, fractional entrainment rate ε , and fractional detrainment rate δ give an internally consistent and closed water budget.

a. Thermodynamic profiles

As shown in appendix B, the constancy of M , RH, and PE implies that ε and δ are equal to each other and proportional to the fractional lapse rate of saturation specific humidity $\gamma = -\partial_z \log(q_v^*)$. Let us define the constant a as $a = \text{PE}\varepsilon/\gamma$. The entrainment rate, detrainment rate, relative humidity, and condensation rate c can then be written as

$$\varepsilon = \delta = \frac{a\gamma}{\text{PE}}, \quad (3)$$

$$\text{RH} = \frac{1 - \text{PE} + a}{1 + a}, \quad \text{and} \quad (4)$$

$$\frac{c}{M} = \frac{\gamma q_v^*}{1 + a}. \quad (5)$$

In these equations, a , PE, RH, and M are constant with height; ε , δ , γ , c , and q_v^* vary with height.

In the zero-buoyancy bulk-plume equations, the environment and the entraining convection (i.e., the zero-buoyancy bulk plume) have identical profiles of temperature $T(z)$ and saturation specific humidity $q_v^*(z)$. As shown in appendix B, these quantities can be combined into a conserved variable:

$$h_a^* = c_p T + gz + \frac{Lq_v^*}{1 + a}, \quad (6)$$

where g is the gravitational acceleration, c_p is the heat capacity of air at constant pressure, and L is the latent heat of condensation, all assumed to be constants. We will refer to h_a^* as the entraining moist static energy (EMSE) of the entraining convection; it is also the saturated EMSE of the environment. This variable is conserved in the sense that it is constant with height for a given a and surface temperature T_s .

Under the assumptions outlined above, the temperature lapse rate Γ can be written as

$$\Gamma = \frac{(1+a)g + (q_v^* L g / R_a T)}{(1+a)c_p + (q_v^* L^2 / R_v T^2)}, \quad (7)$$

where R_a and R_v are the specific gas constants of dry air and water vapor, respectively. Here, and elsewhere, we approximate the specific gas constant of moist air by R_a . For zero entrainment ($a = 0$), the lapse rate of the environment is equal to a moist adiabat, $\text{RH} = 1 - \text{PE}$, and $c = \gamma q_v^* M$. On the other hand, if the entrainment rate is taken to infinity ($a \rightarrow \infty$), the lapse rate of the environment goes to a dry adiabat, $\text{RH} = 1$, and $c = 0$.

Denoting the surface² temperature by T_s , we can approximate the profile of q_v^* as an explicit function of temperature:

$$q_v^*(T) = (1+a) \frac{R_a T_0}{L} W[y_a e^{-f(T_s-T)}], \quad (8)$$

where

$$y_a = \frac{L q_{vs}^*}{(1+a) R_a T_0} \exp\left[\frac{L q_{vs}^*}{(1+a) R_a T_0}\right] \quad \text{and} \quad (9)$$

$$f = \frac{L}{R_v T_0^2} - \frac{c_p}{R_a T_0}. \quad (10)$$

Here, W is the Lambert W function, q_{vs}^* is the saturation specific humidity at the surface, and the constant reference temperature T_0 is chosen below.

We can also obtain an approximate expression for $z(T)$:

$$z(T) = z_s + \frac{c_p}{g} (T_s - T) + \frac{R_a T_0}{g} W(y_a) - \frac{R_a T_0}{g} W[y_a e^{-f(T_s-T)}], \quad (11)$$

² As in R14, we will refer to cloud base as the surface; for a typical cloud-base height of 500 m in RCE, the distinction between cloud base and the surface makes a difference of only 5 K, which is small compared to the range of temperatures we will be exploring. If desired, a boundary layer can be added back to the solutions found in this paper by adding to the “surface” temperatures a temperature increment equal to g/c_p times the cloud-base height.

where z_s is the surface altitude. This equation gives the height of each isotherm in the troposphere. Note that Eqs. (8) and (11) guarantee the conservation of saturated EMSE. Unfortunately, Eq. (11) cannot be inverted to give an analytical expression for $T(z)$, but we will see that $z(T)$ is sufficient to calculate CAPE.

b. Derivation of CAPE

Before we can calculate CAPE, we must first decide where the top of the troposphere is. For this, we will use the fixed-anvil temperature (FAT) hypothesis of Hartmann and Larson (2002). The FAT hypothesis proposes that the temperature at the top of the convecting troposphere remains relatively constant as the surface temperature is changed. Support for this hypothesis has been found from studies of surface temperature changes in both cloud-resolving simulations and global climate models (Kuang and Hartmann 2007; Zelinka and Hartmann 2010; Harrop and Hartmann 2012; Singh and O’Gorman 2015). For lack of an alternative, we will assume that FAT is strictly obeyed over a wide range of surface temperatures, with the tropopause temperature set to 200 K. And, for simplicity, we will assume that the lower stratosphere is isothermal at this temperature.

CAPE is given by the integral over height of the buoyancy of a nonentraining parcel from z_s to its level of neutral buoyancy. In this calculation, we will approximate the nonentraining parcel’s moist static energy (MSE) as being conserved during this ascent; this neglects the small correction from the fact that MSE decreases with height by an amount equal to the parcel’s buoyancy (Romps 2015). The temperature profile of the nonentraining parcel is then given by Eq. (11) with a set to zero. Finally, we will ignore virtual effects and approximate the buoyancy as $g\Delta T/T_0$. With these approximations, CAPE is equal to g/T_0 times the area between the two temperature profiles. This can be written as

$$\text{CAPE} = \frac{g}{T_0} \int_{T_{\text{FAT}}}^{T_s} dT [z_0(T) - z_a(T)],$$

where $T_{\text{FAT}} = 200 \text{ K}$, $z_a(T)$ is given by Eq. (11) with $a > 0$ (i.e., the height as a function of temperature for the environment, the thermal structure of which is set by entraining clouds), and $z_0(T)$ is given by Eq. (11) with $a = 0$ (i.e., the height as a function of temperature for a nonentraining cloud). The right-hand side can be integrated analytically, yielding

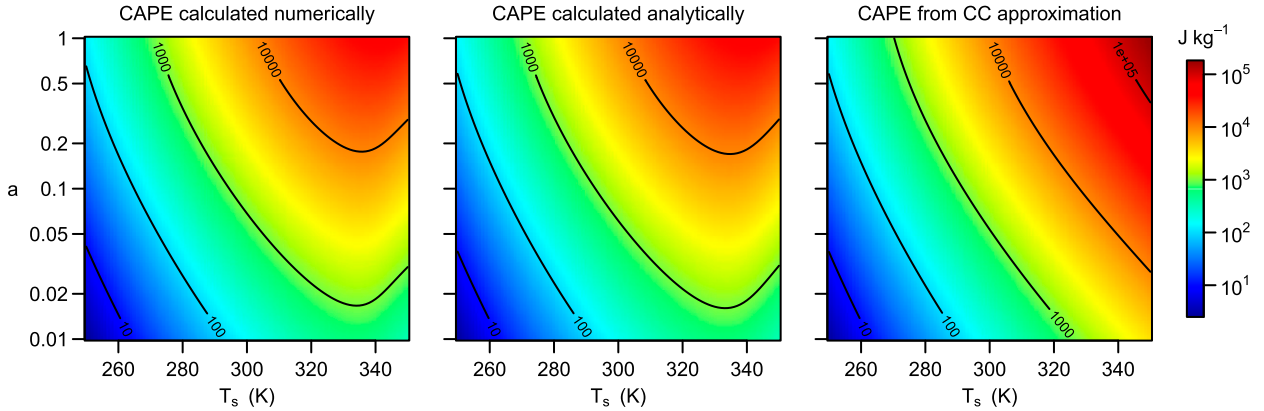


FIG. 1. Plots of CAPE as a function of surface temperature T_s and $a = \text{PE}\epsilon/\gamma$ as calculated from (left) numerical integration of Eq. (B13), (center) the full analytical Eq. (12), and (right) the approximate analytical Eq. (17).

$$\text{CAPE} = \frac{R_a}{2f} \left\{ W(y_a) \left[2 - 2f(T_s - T_{\text{FAT}}) + W(y_a) \right] - W(e^{-f(T_s - T_{\text{FAT}})} y_a) \left[2 + W(e^{-f(T_s - T_{\text{FAT}})} y_a) \right] - W(y_0) \left[2 - 2f(T_s - T_{\text{FAT}}) + W(y_0) \right] + W(e^{-f(T_s - T_{\text{FAT}})} y_0) \left[2 + W(e^{-f(T_s - T_{\text{FAT}})} y_0) \right] \right\}, \quad (12)$$

where y_0 is given by Eq. (9) with $a = 0$. To make T_0 as representative as possible of the mean temperature experienced between the surface and the tropopause, we use $T_0 = (T_s + T_{\text{FAT}})/2$ here and in all of the preceding equations. Although Eq. (12) is a complicated-looking expression, we will see in section 3d that it simplifies dramatically for a wide range of surface temperatures that includes the current tropics.

3. Results

The goals of this section are twofold: to validate the accuracy of these analytical solutions and to explore their implications. In the derivation of Eqs. (8), (11), and (12) for $q^*(T)$, $z(T)$, and CAPE, several simplifying approximations are used. The specific gas constant for moist air is approximated as R_a , T is replaced with an effective temperature T_0 in several places, L is approximated as a constant, and c_p is approximated by the constant value for dry air. In the figures to follow, results labeled “analytical” have been derived using these approximations. Results labeled “numerical” have been calculated numerically by integrating the governing equation for MSE—Eq. (B13) in appendix B—with ϵ varying with height to maintain a constant a for entraining updrafts and with $\epsilon = 0$ for nonentraining updrafts. In the numerical calculations, the heat capacity, gas constant, latent enthalpy, and saturation specific humidity are treated with the full thermodynamics for dry air, vapor, and liquid (Romps 2008, 2015), and saturation is maintained at each height through use of a root solver.

a. Magnitude of CAPE

Equation (12) gives the analytical expression for CAPE as a function of two variables: T_s and a . Note that CAPE does not have any dependence on PE other than through its dependence on a . This invariance can be confirmed by varying PE in numerical integrations of Eq. (B13) while keeping a fixed. The left panel of Fig. 1 shows this numerically calculated CAPE for surface temperatures T_s ranging from 250 to 350 K and for a ranging logarithmically from 0.01 to 1. Note that CAPE increases with a . Recalling that $a = \text{PE}\epsilon/\gamma$, this is to be expected: an increase in the entrainment rate should steepen the environmental lapse rate and, therefore, increase CAPE. Note that CAPE increases with warming over most of this temperature range but not at high temperatures. This behavior will be discussed in section 3f.

We are now in a position to determine a and PE. For the deeply convecting tropics, the ocean temperature is about 300 K, and a typical value of CAPE is about 2000–3000 J kg^{-1} (Williams and Renn 1993). From the numerical results shown in the left panel of Fig. 1, we see that this corresponds to $a = 0.2$. This value of a will be used henceforth. We can estimate PE by referring to studies that have reported the precipitation efficiency from cloud-resolving simulations of deep convection. From a sampling of such studies, the reported efficiencies are 30%–50% (Weisman and Klemp 1982), 36%–42% (Lipps and Hemler 1986), 20%–50% (Ferrier et al. 1996), 27% (Pauluis and Held 2002b), 32%–45% (Tao et al. 2004), 21% (Romps 2011), and

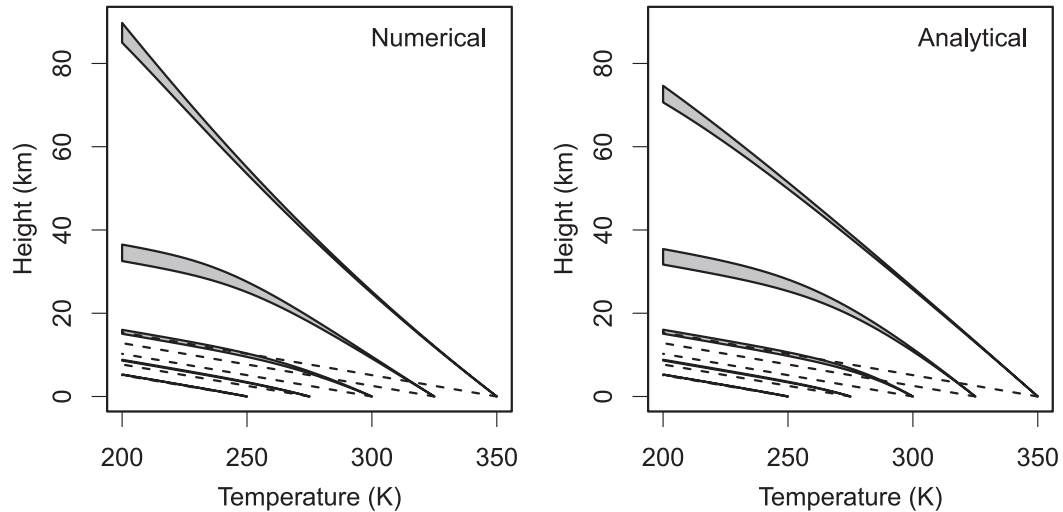


FIG. 2. (left) For surface temperatures of $T_s = 250, 275, 300, 325$, and 350 K , profiles of environmental and nonentraining-parcel temperature profiles calculated by numerical integration of Eq. (B13) (solid) and dry adiabats (dashed). (right) As in (left), but calculated using the analytical expression in Eq. (11). Note that CAPE is proportional to the shaded area between the two temperature profiles.

33%–39% (Langhans et al. 2015). These results indicate that PE lies in the range of 20%–50%. We will split this difference and assign PE a value of 0.35.

What relative humidity and entrainment rate do $a = 0.2$ and $\text{PE} = 0.35$ imply? By Eq. (4), these values imply a relative humidity of about 70%. For the entrainment rate, the answer to this question depends on the value of γ , since $\varepsilon = a\gamma/\text{PE}$. For a surface temperature of 300 K , the water vapor scale height $1/\gamma$ is about 8 km at the surface and roughly halves for every 5 km of elevation (i.e., $1/\gamma = 4\text{ km}$ at $z = 5\text{ km}$, $1/\gamma = 2\text{ km}$ at $z = 10\text{ km}$, and $1/\gamma = 1\text{ km}$ at $z = 15\text{ km}$). For a constant a , this height dependence of γ implies that ε must increase with height. In section 4, we will compare constant- ε solutions to the constant- a solutions studied in this section. For now, however, we simply note that our choices of a and PE give reasonable values of ε . In the midtroposphere, where $1/\gamma \approx 3\text{ km}$, our chosen values of a and PE imply that $\varepsilon \approx 0.2\text{ km}^{-1}$. This is consistent with, but at the low end of, the range of bulk-plume entrainment rates calculated for passive tracers in large-eddy simulations of deep convection (Romps 2010, 2014b).

The center panel of Fig. 1 shows CAPE as calculated from the analytical expression in Eq. (12). Despite using many simplifying approximations, the analytical CAPE is in excellent agreement with the numerical CAPE. The right panel, which obviously differs from the left and center panels, will be discussed in section 3d.

b. CC scaling of tropopause height

We can calculate temperature profiles either numerically by integrating Eq. (B13) or analytically with

Eq. (11). The solid lines in the left panel of Fig. 2 show the environmental temperature profiles and the nonentraining parcel temperatures for five different surface temperatures: 250, 275, 300, 325, and 350 K. For each surface temperature, the gray area between the two curves is proportional to CAPE. Recall that, in accordance with the FAT hypothesis, we use a fixed tropopause temperature of 200 K , and the environmental temperature is assumed to be isothermal above the tropopause. For reference, the dashed lines indicate the dry adiabats.

The right panel of Fig. 2 plots the same information, but as calculated using the analytical expression in Eq. (11). Note the excellent agreement between the two panels. Only for a surface temperature of 350 K does the analytical solution begin to exhibit noticeable departures from the numerical solution.

It is interesting to note that the tropopause height appears to grow exponentially with surface temperature in Fig. 2. To understand why this occurs, we can appeal to EMSE, which was defined in Eq. (6). Using conservation of EMSE and the smallness of q_v^* in the upper troposphere relative to q_{vs}^* , we can approximate the tropopause height z_{FAT} as

$$z_{\text{FAT}} \approx z_s + \frac{c_p}{g}(T_s - T_{\text{FAT}}) + \frac{Lq_{vs}^*}{g(1+a)}. \quad (13)$$

For $T_s = 300\text{ K}$, $T_{\text{FAT}} = 200\text{ K}$, and $z_s = 0\text{ m}$, this gives $z_{\text{FAT}} \approx 15\text{ km}$, with 10 km coming from the difference in dry enthalpy between the surface and the tropopause (middle term on the right-hand side) and 5 km coming

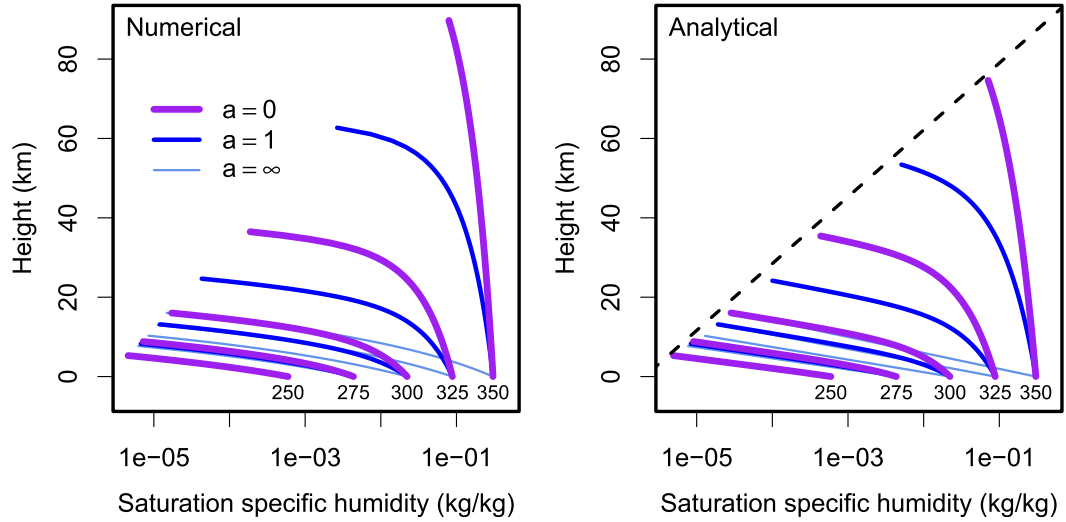


FIG. 3. (left) Profiles of saturation specific humidity q_v^* for five different surface temperatures of $T_s = 250, 275, 300, 325$, and 350 K and three different values of a ($0, 1$, and ∞) calculated by numerical integration of Eq. (B13). (right) As in (left), but calculated using the analytical expression in Eq. (8). The dashed line shows Eq. (13) using $T_0 = 250\text{ K}$ and $T_{s0} = 300\text{ K}$.

from the difference in moist enthalpy between the surface and the tropopause (last term on the right-hand side). Since z_s , c_p , T_{FAT} , L , g , and a are constants, z_{FAT} grows with warming by virtue of two terms: the piece linear in T_s and the piece that is linear in q_{vs}^* . For sufficiently large T_s , the q_{vs}^* piece dominates, giving rise to Clausius–Clapeyron scaling of tropopause-height increases. Using the Clausius–Clapeyron relation for q_{vs}^* , we can calculate the change in tropopause height per degree of surface temperature:

$$\frac{d}{dT_s} z_{\text{FAT}} \approx \frac{c_p}{g} + \frac{L^2 q_{vs}^*}{g R_v T_s^2 (1+a)}. \quad (14)$$

For the surface temperature of the current tropics ($T_s \approx 300\text{ K}$), this predicts $dz_{\text{FAT}}/dT_s = 400\text{ m K}^{-1}$, with 100 m K^{-1} coming from increases in the sensible-enthalpy difference and 300 m K^{-1} coming from increases in the latent-enthalpy difference. For very warm surface temperatures ($320 < T_s < 340\text{ K}$), the tropopause height becomes extraordinarily sensitive to surface temperature with dz_{FAT}/dT_s in the range of $1\text{--}2\text{ km K}^{-1}$. Because of the smallness of a ($a \approx 0.2$), these predictions are very similar to the predictions obtained using MSE (i.e., EMSE with $a = 0$).

For the $T_s = 350\text{ K}$ case, note in Fig. 2 that the lapse rate does not asymptote to the dry adiabatic lapse rate in the upper troposphere. This is caused by the substantial upper-tropospheric specific humidity ($q_v^* \approx 0.05$ at the tropopause), which is related to the super-CC scaling of tropopause specific humidity discussed below. The

noticeable *decrease* in lapse rate with height in the numerical solution of $T_s = 350\text{ K}$ stems from the explicit instances of T in the lapse-rate equation:

$$\Gamma = \frac{(1+a)g + (q_v^* L g / R_a T)}{(1+a)c_p + (q_v^* L^2 / R_v T^2)}.$$

The analytical theory sets those explicit instances of T to a constant T_0 , so the analytical theory does not capture this effect.

c. Super-CC scaling of stratospheric humidity

We will now take a look at q_v^* profiles and explore how they change with surface temperature. The left panel of Fig. 3 shows profiles of q_v^* for five different surface temperatures of $T_s = 250, 275, 300, 325$, and 350 K and three different values of a : $a = 0$ (the nonentraining parcel), $a = 1$, and $a = \infty$ (corresponding to the dry adiabat). Noting that the abscissa is a log axis, we see that the surface saturation humidity q_{vs}^* obeys Clausius–Clapeyron scaling, increasing roughly exponentially with surface warming. The value of q_v^* in the tropopause, however, appears to increase even more rapidly than q_{vs}^* at warm surface temperatures, which would indicate super-CC scaling. Another curiosity is the apparently linear relationship between the height of the tropopause and the logarithm of q_v^* at the tropopause.

We can understand all of these features by examining the analytical solutions given by Eq. (8), which are plotted in the right panel of Fig. 3. In the upper troposphere, q_v^* is typically small enough that $Lq_v^* \ll R_a T_0$.

For example, in the current tropics, Lq_v^* at the tropopause is several orders of magnitude smaller than $R_a T_0$. In Eq. (8), this implies that the W function has a value much less than one, so it may be approximated by its argument. Therefore, in the upper troposphere, we may approximate q_v^* as

$$q_v^*(T) = \frac{R_a}{R_v} \frac{p_v^*(T)}{p_s} \exp \left[\frac{c_p}{R_a T_0} (T_s - T) + \frac{Lq_{vs}^*}{(1+a)R_a T_0} \right] \\ (\text{upper troposphere}), \quad (15)$$

where p_s is the surface pressure. For $T = T_{\text{FAT}}$, the term in front of the exponential is constant, and $q_v^*(T_{\text{FAT}})$ scales as the exponential of the sum of two terms: a term linear in T_s and a term linear in q_{vs}^* . We can also arrive at Eq. (15) by using $q_v^* = R_a p_v^*/R_v p$ along with the expression for $p(T)$ given in appendix B. Since $p_v^*(T_{\text{FAT}})$ is invariant with surface warming, the growth of $q_v^*(T_{\text{FAT}})$ with T_s is entirely due to the decrease in tropopause pressure as the troposphere deepens with warming.

Since the Brewer–Dobson circulation pegs the humidity of the tropical lower stratosphere to the saturation specific humidity at the tropopause (Brewer 1949), this expression tells us how stratospheric humidity depends on surface temperature. Using Eq. (15) to calculate the fractional change in $q_v^*(T_{\text{FAT}})$ per degree of surface warming, we find

$$\frac{d}{dT_s} \log[q_v^*(T_{\text{FAT}})] = \frac{c_p}{R_a T_0} + \frac{L}{R_v T_s^2} \frac{Lq_{vs}^*}{(1+a)R_a T_0}.$$

The first term ($c_p/R_a T_0$) is only about $1\% \text{ K}^{-1}$. The second term is the CC-scaling rate ($L/R_v T_s^2$) times the ratio $Lq_{vs}^*/[(1+a)R_a T_0]$. Therefore, we have sub-CC scaling of stratospheric humidity when $Lq_{vs}^*/[(1+a)R_a T_0] \leq 1$ and super-CC scaling of stratospheric humidity when $Lq_{vs}^*/[(1+a)R_a T_0] \geq 1$. For $a = 0.2$, the transition from sub-CC scaling to super-CC scaling occurs around $T_s \approx 304 \text{ K}$. Above this temperature, surface warming causes stratospheric specific humidity to grow faster (in a fractional sense) than near-surface specific humidity.

The top row of Fig. 4 plots the tropopause q_v^* as a function of surface temperature for three values of a using, from left to right: numerical integration, Eq. (8) evaluated at $T = T_{\text{FAT}}$, and Eq. (15) evaluated at $T = T_{\text{FAT}}$. Equation (15) deviates from the numerical and full analytical solutions only at very warm surface temperatures, where q_v^* at the tropopause is not small enough to satisfy $Lq_v^* \ll R_a T_0$. The bottom row of Fig. 4 plots the fractional increase in tropopause q_v^* per kelvin of surface warming. Note that the $a = 0.2$ curve would be very close to the thick, purple, $a = 0$ curve on this plot (and, therefore, is not plotted to avoid

clutter). For $T_s = 300 \text{ K}$, these results predict that tropical lower-stratospheric humidity increases at a rate of about 6% per kelvin of surface warming. This rate of increase is smaller for colder temperatures (e.g., about $3\% \text{ K}^{-1}$ for $T_s = 275 \text{ K}$) and larger for warmer temperatures (e.g., about $15\% \text{ K}^{-1}$ for $T_s = 325 \text{ K}$, and reaching as high as $30\% \text{ K}^{-1}$). Also shown in the left panels of Fig. 4 are the $q_v^*(200 \text{ K})$ and their rates of exponential increase from the two sets of large-eddy simulations presented by R14. For consistency with the neglect of ice in the derivations here, values of $q_v^*(200 \text{ K})$ are calculated with respect to liquid; the ratio of liquid and ice partial pressures at 200 K is approximately 2, and this ratio is independent of surface temperature. Those simulations were run to RCE over fixed sea surface temperatures of $290, 300, 310$, and 320 K , and their $q_v^*(200 \text{ K})$ values exhibit the behavior predicted here: namely, the transition from sub-CC scaling to super-CC scaling.

Finally, we can explain the apparently linear relationship between z_{FAT} and the logarithm of tropopause q_v^* . Evaluating Eq. (15) at $T = T_{\text{FAT}}$ and then using Eq. (13) to eliminate q_{vs}^* in the exponential, we get

$$q_v^*(T_{\text{FAT}}) = \frac{R_a}{R_v} \frac{p_v^*(T_{\text{FAT}})}{p_s} \exp \left[\frac{g}{R_a T_0} (z_{\text{FAT}} - z_s) \right]. \quad (16)$$

Since $p_v^*(T_{\text{FAT}})$ and p_s are independent of T_s , we see that $q_v^*(T_{\text{FAT}})$ goes as the exponential of z_{FAT} . Equivalently, there is a linear relationship between the height of the tropopause and the logarithm of the tropopause q_v^* . The dashed line in Fig. 3 plots Eq. (16) using $T_0 = 250 \text{ K}$.

d. CC scaling of CAPE

The original question posed in section 1 is whether or not CAPE exhibits CC scaling. Indeed, inspection of Eq. (12) reveals that there is a wide range of temperatures for which CAPE scales as q_{vs}^* . For $Lq_{vs}^* \ll R_a T_0$ and $T_s - T_{\text{FAT}} \geq 2/f \approx 20\text{--}30 \text{ K}$, we know that $W[e^{-f(T_s - T_{\text{FAT}})} y_a] \ll W(y_a) \ll 1$, so we can safely approximate Eq. (12) as

$$\text{CAPE} = \frac{R_a}{2f} \left\{ W(y_a) [2 - 2f(T_s - T_{\text{FAT}})] - W(y_0) [2 - 2f(T_s - T_{\text{FAT}})] \right\}.$$

Since the Lambert W function is defined by $W(xe^x) = x$, and since y_a is given by Eq. (9), this simplifies to

$$\text{CAPE} = \frac{a}{1+a} \frac{Lq_{vs}^*}{T_0} (T_s - T_{\text{FAT}} - T_c), \quad (17)$$

where

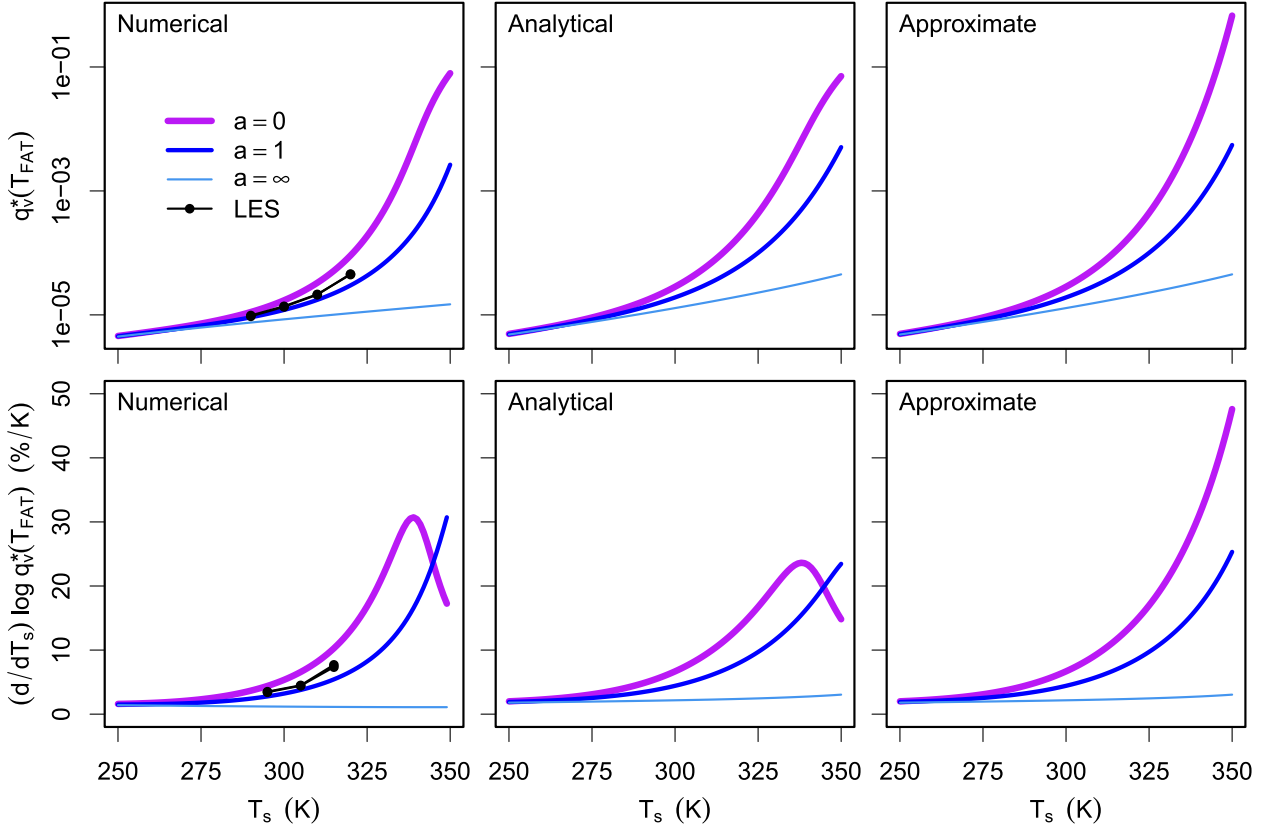


FIG. 4. (top) The tropopause q_v^* as a function of surface temperature T_s for three different values of a (0, 1, and ∞), as calculated (left) numerically, (center) analytically from Eq. (8) using $T = T_{FAT}$, and (right) analytically using Eq. (15) with $T = T_{FAT}$. The black circles show the mean q_v^* (with respect to liquid) at $T = 200$ K in the large-eddy simulations of R14. (bottom) As in (top), but for the fractional increase in tropopause q_v^* per kelvin of surface warming.

$$T_c = \frac{R_a T_0}{(R_a L/R_v T_0) - c_p} = O(10) \text{ K}. \quad (18)$$

In this expression for CAPE, there is a relatively weak linear dependence on an explicit T_s . Most of the variation in CAPE comes from the fact that it is proportional to the surface saturation humidity q_{vs}^* .

Figure 5 plots Eq. (17) as the dotted red line, along with the numerical solution and the full analytical solution from Eq. (12). The two panels of Fig. 5 display the same information, but the ordinate is linear in the left panel and logarithmic in the right panel. Clearly, the three curves are in excellent agreement up to a surface temperature (really, cloud-base temperature) of about 310 K. In other words, CAPE exhibits CC scaling over temperatures ranging from less than 250 K all the way up to 310 K. This behavior is also evident in Fig. 1, which plots Eq. (17) in the right panel for comparison with the other two.

What sets the temperature at which CAPE deviates from CC scaling? In the derivation of Eq. (17), we used the assumption that $Lq_{vs}^* \ll R_a T_0$. Deviations from CC

scaling are to be expected, therefore, around the T_s where $Lq_{vs}^* \approx R_a T_0$. This equality occurs at about $T_s = 310$ K, at which q_{vs}^* is equal to 0.04. Figure 6 illustrates the departure from CC scaling at this temperature. Plotted in Fig. 6 is the fractional increase in CAPE per degree of surface warming calculated using the approximate CC scaling from Eq. (17) in red and the full analytical solution from Eq. (12) in blue (for $0 < a < \infty$). For the current tropics, both the full analytical solution and the approximate CC-scaling solution agree that CAPE should increase by about 6%–7% K⁻¹. The thin vertical line marks the temperature at which $Lq_{vs}^* = R_a T_0$; this separates the CC-scaling regime on the left from the non-CC-scaling regime on the right.

It is worth noting that Eq. (17) can be recast in terms of RH and PE. Since $RH = (1 - PE + a)/(1 + a)$, we can write a as $a = PE/(1 - RH) - 1$. Therefore, Eq. (17) can be written as

$$\text{CAPE} = \left(1 - \frac{1 - RH}{PE}\right) \frac{Lq_{vs}^*}{T_0} (T_s - T_{FAT} - T_c). \quad (19)$$

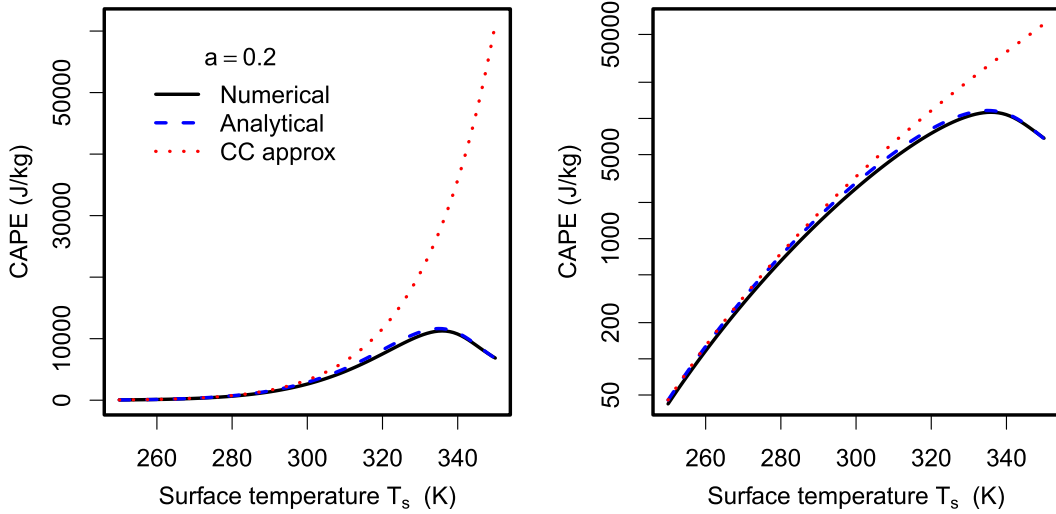


FIG. 5. (left) CAPE as a function of surface temperature T_s for $a = 0.2$, as calculated using numerical integration (black solid), the analytical expression for CAPE given by Eq. (12) (blue dashed), and the approximate analytical expression for CAPE in Eq. (17) (red dotted), which exhibits CC scaling. (right) As in (left), but with a log axis.

For PE less than $1 - \text{RH}$, this equation appears to predict negative CAPE, which would be nonsense. As shown by R14, however, PE is always greater than or equal to $1 - \text{RH}$, so CAPE is always nonnegative. The veracity of $\text{PE} \geq 1 - \text{RH}$ can also be seen from the equations presented in this paper: since $a \equiv \text{PE}\varepsilon/\gamma$ is manifestly nonnegative, and since $a = \text{PE}/(1 - \text{RH}) - 1$, the inequality must hold.

To get a sense for the parcel buoyancies that are responsible for generating these CAPE values, Fig. 7 plots the buoyancies of nonentraining parcels lifted through an atmosphere with $a = 0.2$. The left panel shows the numerical results, and the right panel shows the results obtained using analytical Eq. (11) for the environment ($a = 0.2$) and the nonentraining parcel ($a = 0$). It is noteworthy that, for a given surface temperature, the largest buoyancies are in the upper troposphere. This occurs despite the absence of ice processes here; this is consistent with the explanation of this behavior given by Seeley and Romps (2015b). It is also noteworthy that the largest overall buoyancies occur for a surface temperature of about 325 K instead of at the largest surface temperature of 350 K.

e. Why does CAPE exhibit CC scaling?

The best way to gain an intuition for Eq. (17) is to rederive it using the conservation of saturated EMSE. The troposphere has a constant saturated EMSE h_a , the value of which can be written either in terms of T , $z(T)$, and $q_v^*(T)$ (left-hand side) or in terms of T_s , z_s , and q_{vs}^* (right-hand side):

$$c_p T + gz(T) + \frac{Lq_v^*(T)}{1+a} = c_p T_s + gz_s + \frac{Lq_{vs}^*}{1+a}. \quad (20)$$

An undiluted parcel lifted from the surface will have a constant EMSE h_0 , the value of which can be written either in terms of T' , $z(T')$, and $q_v^*(T')$ (left-hand side) or in terms of T_s , z_s , and q_{vs}^* (right-hand side):

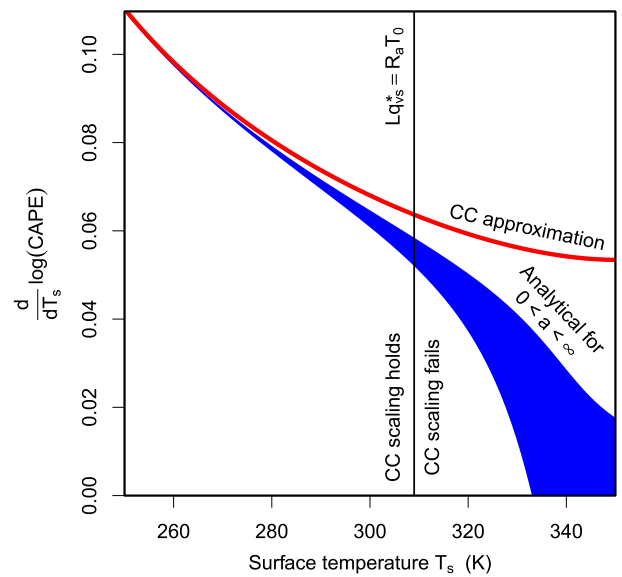


FIG. 6. The fractional increase in CAPE per degree of surface warming calculated using the approximate Eq. (17) (red), which exhibits CC scaling, and Eq. (12) plotted for the full range of possible a (blue). The thin vertical line marks the temperature at which $Lq_{vs}^* = R_a T_0$.

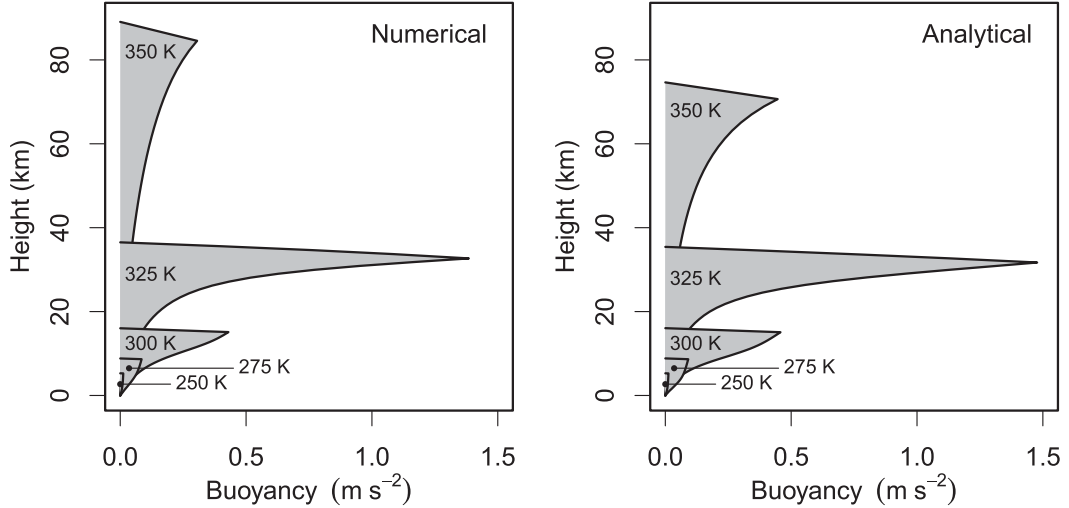


FIG. 7. The buoyancy profiles for nonentraining parcels lifted through atmospheres with $a = 0.2$ and surface temperatures of $T_s = 250, 275, 300, 325$, and 350 K and calculated using (left) numerical integration and (right) Eq. (11).

$$c_p T' + gz(T') + Lq_v^*(T') = c_p T_s + gz_s + Lq_{vs}^*. \quad (21)$$

At the same height z , the temperature T' of the undiluted parcel will exceed the temperature T of the environment; let us denote this difference by $\Delta T \equiv T' - T$. Subtracting Eq. (20) from Eq. (21) at the same height z , we get

$$c_p \Delta T + Lq_v^*(T + \Delta T) - \frac{Lq_v^*(T)}{1+a} = \frac{a}{1+a} Lq_{vs}^*.$$

This equation says that, at a height z , the difference in EMSE between the undiluted parcel and the environment (left-hand side) is equal to a constant (right-hand side). Taylor expanding $q_v^*(T + \Delta T)$ to first order around T and using the Clausius–Clapeyron equation, this can be solved for ΔT and then written in terms of buoyancy $b = g\Delta T/T$:

$$b = \frac{a}{1+a} \frac{gL}{T} \frac{q_{vs}^* - q_v^*}{c_p + (L^2 q_v^*/R_v T^2)}.$$

Note that this expression for b depends on q_v^* in both the numerator and denominator.

Let us now consider atmospheres that satisfy $q_{vs}^* L \ll R_a T_s$; on Earth, this condition is satisfied for surface temperatures below about 310 K. If this condition is met, then we know that $q_v^* L \ll R_a T$ throughout the troposphere, because q_v^* decreases more rapidly with height than T . In this regime, the lapse rate for an undiluted parcel is given by Eq. (7), with $a = 0$ and the numerator equal to g :

$$\Gamma = \frac{g}{c_p + (L^2 q_v^*/R_v T^2)}.$$

To calculate CAPE, we are interested in bdz , which is the specific work done by buoyancy in the height interval dz . Up to a sign, this can be written as $(b/\Gamma)dT$, which is the specific work done by buoyancy in the temperature interval dT . When we divide b by Γ , note that their denominators cancel, leading to

$$\frac{b}{\Gamma} = \frac{a}{1+a} \frac{L}{T} (q_{vs}^* - q_v^*). \quad (22)$$

This simple expression tells us the specific work per temperature interval.

Equation (B20) in appendix B gives the differential equation that relates the profile of q_v^* to the profile of T . For $q_v^* L \ll R_a T$, that equation tells us that the q_v^* profile has an exponential dependence on temperature with an e folding for every temperature increment T_c , which is the constant given by Eq. (18). In other words, $q_v^* = q_{vs}^* \exp[(T - T_s)/T_c]$ throughout the troposphere. Therefore, the profiles of buoyancy b and the specific work per temperature interval b/Γ simplify to

$$b = \frac{a}{1+a} \frac{gLq_{vs}^*}{T} \frac{1 - e^{(T-T_s)/T_c}}{c_p + (L^2 q_{vs}^*/R_v T^2) e^{(T-T_s)/T_c}} \quad \text{and} \quad (23)$$

$$\frac{b}{\Gamma} = \frac{a}{1+a} \frac{Lq_{vs}^*}{T} [1 - e^{(T-T_s)/T_c}]. \quad (24)$$

Approximating the T in the denominator by T_0 and then integrating Eq. (24) over temperature from T_{FAT} to T_s while noting that $T_s - T_{\text{FAT}} \gg T_c$, we get an expression for CAPE:

$$\text{CAPE} = \frac{a}{1+a} \frac{Lq_{vs}^*}{T_0} (T_s - T_{\text{FAT}} - T_c).$$

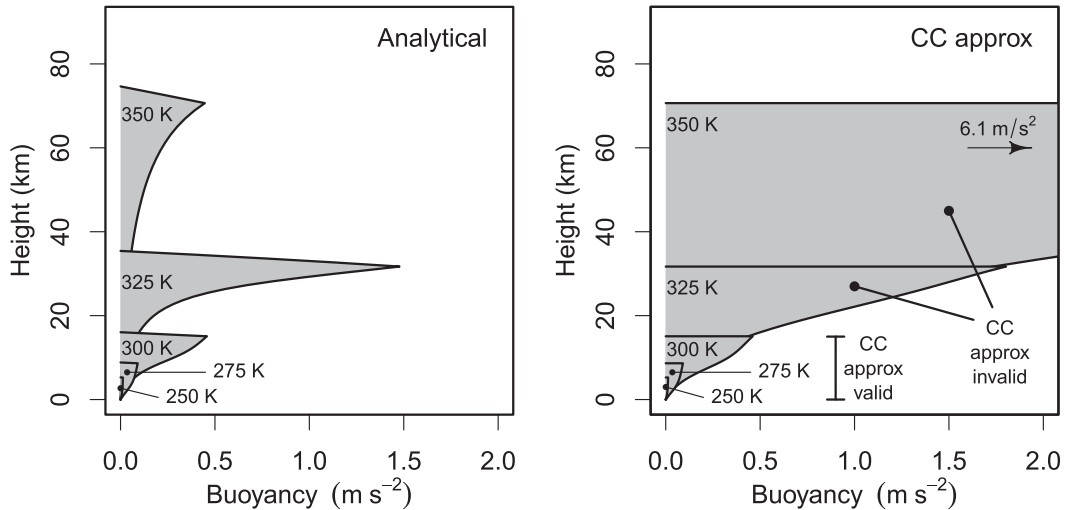


FIG. 8. As in Fig. 7, but using (left) Eq. (11) and (right) Eq. (23).

This is exactly the same as Eq. (17). Note that we used the condition $q_{vs}^* L \ll R_a T_s$ twice in this derivation: to simplify Γ and to write q_v^* as an exponential function of T . Therefore, this expression for CAPE should fail when $q_{vs}^* L \ll R_a T_s$ ceases to be true, which occurs for surface temperatures greater than about 310 K.

From this derivation, we see that the CC scaling of CAPE is driven by the CC scaling of work per temperature interval, b/Γ . From Eq. (24), b/Γ is proportional to q_{vs}^* (CC scaling) times a function of temperature that transitions from zero at the surface to approximately one at and above the $T_s - T_c$ isotherm. Therefore, CAPE scales as q_{vs}^* times the temperature range $T_s - T_c - T_{FAT}$. The fact that the temperature range increases with T_s adds an additional $\sim 1\% \text{ K}^{-1}$ growth in CAPE with surface warming.

The right panel of Fig. 8 illustrates the simple buoyancy profiles described by Eq. (23). The areas under these buoyancy curves are equal to the values given by Eq. (17) and plotted as the dotted red curve in Fig. 5. The added value of Fig. 8 is that it allows us to see how the failure of CAPE CC scaling (for $T_s \gtrsim 310 \text{ K}$) is expressed in the corresponding buoyancy profiles. As expected, Eq. (23) produces accurate buoyancy profiles for surface temperatures of 250, 275, and 300 K. For surface temperatures of 325 and 350 K, Eq. (23) dramatically errs in predicting the buoyancy, which is the expected behavior because surface temperatures of 325 and 350 K are above the $\sim 310\text{-K}$ cutoff for the CC scaling of CAPE.

f. Why does CAPE peak around $T_s \approx 335 \text{ K}$?

In Fig. 5, we see that CAPE peaks at $T_s \approx 335 \text{ K}$. To understand why, we must first note that the temperature

anomaly ΔT (relative to the environment at the same height) of an undiluted parcel lifted from the surface is related to its saturated MSE anomaly Δh^* by an approximate linear relation:

$$\Delta h^* \approx \beta \Delta T, \quad (25)$$

where

$$\beta = c_p + L \frac{\partial q_v^*}{\partial T} = c_p + \frac{q_v^* L^2}{R_v T^2}. \quad (26)$$

If $q_v^* L^2 / R_v T^2 > c_p$, then the saturated MSE difference between an undiluted parcel and its environment is expressed mostly as a latent enthalpy anomaly (i.e., as a q_v^* anomaly). If $q_v^* L^2 / R_v T^2 < c_p$, then the saturated MSE difference between an undiluted parcel and its environment is expressed mostly as a sensible-enthalpy anomaly (i.e., as a T anomaly). The altitude where $q_v^* L^2 / R_v T^2 = c_p$ (i.e., where $\beta = 2c_p$) serves as a natural divider between these two regimes.

Seeley and Romps (2016) explained how convective entrainment and Eq. (25) give rise to the “shape of CAPE.” In the lower troposphere, the buoyancy of an undiluted parcel grows with height because the saturated MSE difference Δh^* between the undiluted parcel and its environment grows with height. Although Δh^* grows with height, it tends to plateau above one water vapor scale height since the MSE-reducing effect of entrainment is proportional to the subsaturation of the environment, $(1 - \text{RH})q_v^*$.

On the other hand, the buoyancy profile of an undiluted parcel (i.e., the shape of CAPE) is much more top-heavy, and this is caused by the dependence of β on

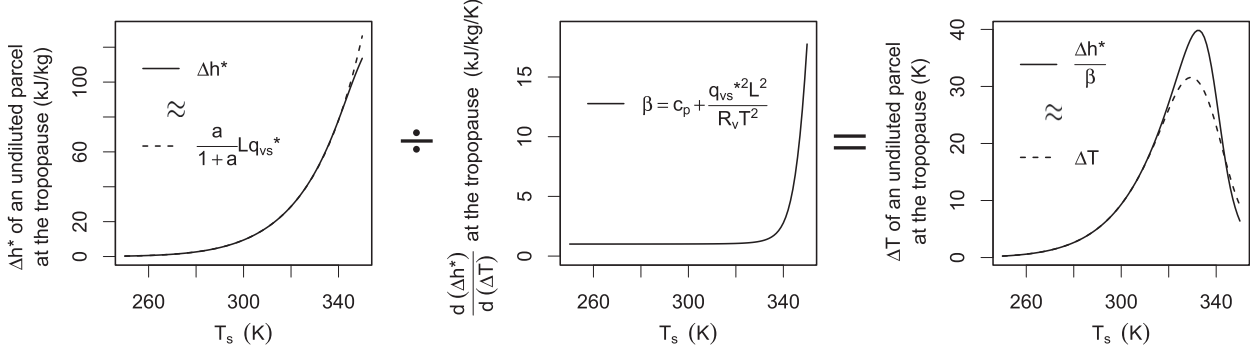


FIG. 9. (left) The saturated MSE anomaly Δh^* of an undiluted parcel lifted to the tropopause as a function of T_s , calculated from the analytical Eqs. (8)–(11) (solid) and the approximation for Δh^* given by Eq. (27) (dashed). (center) The value of β , defined by Eq. (26), at the tropopause as a function of T_s . (right) The ratio $\Delta h^*/\beta$, which approximates the temperature anomaly ΔT of the undiluted parcel (solid), and the actual temperature anomaly ΔT , calculated from the analytical Eq. (11) (dashed).

q_v^* . In the lower troposphere, where $\beta > 2c_p$, Δh^* is expressed primarily as a latent enthalpy difference, so ΔT is suppressed. In the upper troposphere, where $\beta < 2c_p$, Δh^* is expressed primarily as a sensible-enthalpy difference, so ΔT is enhanced. This leads to the prominent and familiar reservoir of large buoyancy in the upper troposphere. A common misconception is that the latent heat of fusion is responsible for this large upper-tropospheric buoyancy. This misconception has been fueled by the coincidence that, in Earth's current tropics, the 273-K isotherm is close to the altitude where $\beta = 2c_p$ (Seeley and Romps 2016).

We are now in a position to understand why CAPE hits its maximum value around $T_s \approx 335$ K. In short, this is the surface temperature at which the $\beta = 2c_p$ surface reaches the tropopause. Once this happens, β exceeds $2c_p$ throughout the troposphere, so the saturated MSE anomaly of an undiluted parcel is never expressed primarily as a sensible-enthalpy anomaly. In other words, Δh^* is never fully expressed as buoyancy.

This is illustrated by Fig. 9. In the left panel, the solid curve plots Δh^* at the tropopause calculated from the analytical Eqs. (8)–(11) using $a = 0.2$ for the environment and $a = 0$ for the undiluted parcel, with a root solver used to find the undiluted-parcel temperature at the tropopause. Note that Δh^* grows roughly exponentially with surface temperature, which we can understand by the fact, shown in appendix C, that

$$\Delta h^*(z_{\text{FAT}}) \approx \frac{a}{1+a} L q_{vs}^*. \quad (27)$$

This approximation for Δh^* is plotted as the dashed curve in the left panel of Fig. 9. Equation (27) tells us that Δh^* at the tropopause exhibits approximate Clausius–Clapeyron scaling with respect to T_s .

The center panel of Fig. 9 plots β at the tropopause using analytical Eq. (8). At the tropopause, β reaches

$2c_p$ at $T_s \approx 335$ K. The temperature anomaly of an undiluted parcel ΔT is given approximately by $\Delta h^*/\beta$, which is plotted as the solid curve in the right panel of Fig. 9. Even though Δh^* grows exponentially throughout this wide range of T_s , the rapid increase of β at $T_s \approx 335$ K causes ΔT to peak there. This is corroborated by the actual tropopause ΔT plotted as the dashed curve in the right panel of Fig. 9, which is found using a root solver as mentioned above.

We can derive $T_s \approx 335$ K as follows. By the definition of β , the $\beta = 2c_p$ surface hits the tropopause when

$$\frac{q_v^*(T_{\text{FAT}})L^2}{R_v T_{\text{FAT}}^2} = c_p.$$

If we combine this with Eq. (15), which gives an expression for q_v^* at the tropopause, then we find that the $\beta = 2c_p$ surface hits the tropopause when the near-surface specific enthalpy ($c_p T_s + L q_{vs}^*$) reaches $c_p T_{\text{FAT}} + R_a T_0 \log[R_v^2 c_p T_{\text{FAT}}^2 p_s / R_a L^2 p_v^*(T_{\text{FAT}})] \approx 0.7 \text{ MJ kg}^{-1}$. This occurs at a T_s of about 335 K.

4. Constant ε

Up to this point, we have exclusively studied solutions with constant a . We have focused on the constant- a cases because they correspond to constant RH (which is attractive for its theoretical simplicity) and because they are analytically soluble. The downside to using constant a is that it implies a z -dependent and T_s -dependent ε .

How might we expect CAPE to change if we used constant ε instead of constant a ? To get a hint, consider a hybrid of these two conditions: make ε at the surface independent of T_s (which makes a at the surface vary as a function of T_s), but hold a fixed at its surface value throughout the troposphere (so that ε varies in the vertical). Since $a = PE\varepsilon/\gamma$, and since the scale height $1/\gamma$

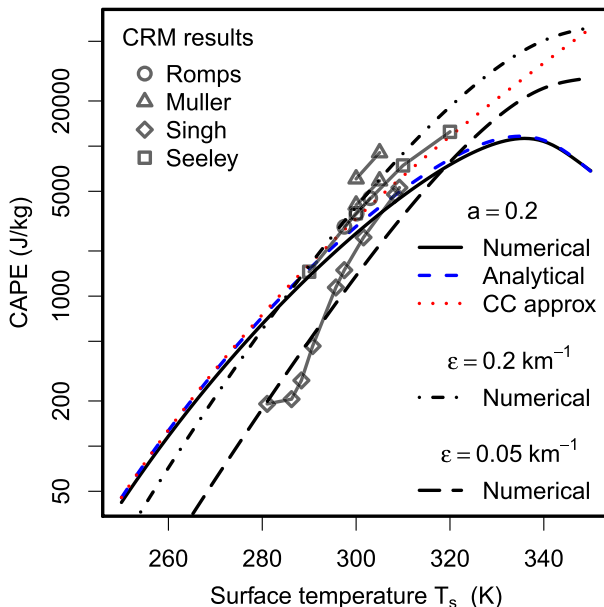


FIG. 10. As in Fig. 5 (right), but with numerical solutions added for $\epsilon = 0.2$ (dotted-dashed) and 0.05 km^{-1} (long dashed) and with data overlaid from the cloud-resolving simulations of Romps (2011) (circles), Muller et al. (2011) (triangles), SO13 (diamonds), and Seeley and Romps (2015b) (squares).

increases at the surface with surface warming, the value of a must increase with surface warming in this scenario. By Eq. (17), an increase in a with warming would cause CAPE to increase faster than it does with constant a . This suggests that CAPE increases somewhat faster with warming when we use constant ϵ than it does when we use constant a .

This may explain why some of the cloud-resolving simulations discussed in section 1 found increases in CAPE that exceed the CC-scaling prediction. As discussed in section 3d, the analytical solutions for CAPE using constant a predict an increase of CAPE in the current tropics by about $6\%-7\text{ K}^{-1}$. Meanwhile, studies of cloud-resolving simulations report increases of 7% (Seeley and Romps 2015b), 8% (Romps 2011; Muller et al. 2011), and 12% K^{-1} (SO13).

Although we do not have analytical constant- ϵ solutions for CAPE, we can calculate CAPE for constant ϵ numerically. Figure 10 replots the right panel of Fig. 5 and adds to it two of these numerical solutions (one for $\epsilon = 0.2 \text{ km}^{-1}$ and one for $\epsilon = 0.05 \text{ km}^{-1}$). We see that, indeed, CAPE with constant ϵ increases somewhat faster than CAPE with constant a . More importantly, using $\epsilon = 0.2 \text{ km}^{-1}$, which is the entrainment rate we had estimated in section 3a as the closest analog to $a = 0.2$, gives CAPE values that are very similar to the $a = 0.2$ solutions, especially below a surface temperature of 310 K. By an apparent coincidence, the increase in

a with warming in the $\epsilon = 0.2\text{-km}^{-1}$ solution causes CAPE to track the CC-scaling approximation better than the constant- a solutions at high temperatures.

Overlaid on Fig. 10 are the CAPE values reported from the studies of RCE in cloud-resolving simulations. The two pairs of values plotted for Muller et al. (2011) correspond to the two different methods they used to calculate CAPE, assuming pseudoadiabatic ascent for one and adiabatic ascent for the other. The CAPE values from Romps (2011), Muller et al. (2011), and Seeley and Romps (2015b) agree fairly well with both the approximate CC-scaling CAPE given in Eq. (17) and with the $\epsilon = 0.2\text{-km}^{-1}$ numerical solutions. This agreement is even more impressive considering that these cloud-resolving model results were obtained from two different models and three different sets of grid spacings and domain sizes. The simulations of SO13, which used yet another cloud-resolving model, appear to more closely track the solution obtained with $\epsilon = 0.05 \text{ km}^{-1}$.

5. Summary

In an effort to understand the workings of convective available potential energy (CAPE), we have derived here the first analytical solutions to radiative-convective equilibrium (RCE). These solutions are given by Eqs. (4), (8), and (11), which specify RH, $q_v^*(T)$, and $z(T)$, respectively. With these, we have derived Eq. (12), which gives an analytical expression for CAPE. We have also confirmed that these analytical solutions closely match the numerical solutions (see Figs. 1–5 and 7).

These solutions lead to several insights about RCE that stand apart from our main focus on CAPE. As shown in section 3b, changes to the tropopause height exhibit Clausius–Clapeyron (CC) scaling at warm temperatures, increasing in proportion to the surface saturation specific humidity q_{vs}^* . At current tropical temperatures, Eq. (14) predicts that the tropopause rises by 400 m for every 1 K of surface warming, but this increases in proportion to q_{vs}^* up to rates of 1–2 km K^{-1} at higher temperatures. In section 3c, we learned that stratospheric humidity exhibits super-CC scaling at warm temperatures. At current tropical temperatures, Eq. (15) evaluated at the tropopause temperature predicts a fractional increase in the humidity of the tropical lower stratosphere of about 6% per kelvin of surface warming, but this increases to as high as 30% K^{-1} at higher temperatures.

Returning to the analytical expression for CAPE, we have found that CAPE is well approximated by Eq. (17), which exhibits CC scaling as a result of the overall factor of q_{vs}^* . This CC scaling of CAPE holds for temperatures up to about 310 K, which corresponds to the temperature

at which $Lq_{vs}^* \approx R_a T_s$. At higher surface temperatures, CAPE falls off of its Clausius–Clapeyron trajectory and even decreases at very warm temperatures (see Fig. 5). As illustrated in Fig. 10, this theory for CAPE agrees well with most of the recent results from cloud-resolving simulations.

Acknowledgments. This work was supported by the Scientific Discovery through Advanced Computing (SciDAC) program funded by the U.S. Department of Energy Office of Advanced Scientific Computing Research and Office of Biological and Environmental Research under Contract DE-AC02-05CH11231. The author is grateful to Jacob Seeley, Martin Singh, and two anonymous reviewers for helpful comments on the manuscript.

APPENDIX A

Derivation of Eq. (2)

We derive here the (incorrect) expression for CAPE postulated in Eq. (2). Let Q_r (W m^{-3}) be the profile of radiative heating (i.e., $Q_r < 0$), and let Q_l (W m^{-3}) be the profile of latent heating (i.e., $Q_l > 0$). Let us define H_l and H_r as the mean heights of these cooling profiles:

$$H_{r,l} = \frac{\int_0^\infty dz z Q_{r,l}}{\int_0^\infty dz Q_{r,l}}.$$

The profile of cloud temperature anomaly ΔT (i.e., the difference in temperature between the cloud and the environment) is given by the conservation of energy at each height:

$$Q_r + Q_l - \partial_z(\bar{M}c_p \Delta T) = 0.$$

Integrating this equation upward in height starting from z , we get

$$\bar{M}c_p \Delta T(z) = - \int_z^\infty dz' [Q_r(z') + Q_l(z')].$$

To connect this to CAPE, we must assume that clouds are nonentraining so that their buoyancies ($g\Delta T/T$) are the same as that of an undiluted parcel. If they are nonentraining, then the mass flux M is constant up to the tropopause height z_t , above which M , Q_l , and Q_r are all zero. Approximating buoyancy as $g\Delta T/T_0$, where T_0 is a representative tropospheric temperature, we can then write CAPE as

$$\begin{aligned} \text{CAPE} &= \int_0^{z_t} dz b(z) \\ &= \int_0^{z_t} dz \frac{g\Delta T(z)}{T_0} \\ &= \frac{g}{Mc_p T_0} \int_0^{z_t} dz Mc_p \Delta T(z) \\ &= -\frac{g}{Mc_p T_0} \int_0^{z_t} dz \int_z^\infty dz' [Q_r(z') + Q_l(z')]. \end{aligned}$$

Using integration by parts, the double integral can be written as $(H_l - H_r)Q$, where $Q = \int_0^\infty dz Q_l = -\int_0^\infty dz Q_r$ is the total radiative cooling (W m^{-2}) of the troposphere. Therefore, we get $M\text{CAPE} = \eta'Q$ with $\eta' = g(H_r - H_l)/c_p T_0$, which is the result given in Eq. (2). Note, however, that this expression for CAPE is incorrect for the reasons discussed in section 1.

APPENDIX B

Derivation of Equations in Section 2

We derive here the equations presented in section 2. Section a of appendix B begins by deriving the temperature lapse rate $\Gamma \equiv -\partial_z T$. With the expression for Γ , section b of appendix B derives the function $q_v^*(T)$, which specifies how saturation specific humidity q_v^* and temperature T covary in height. This expression is then used in appendix B, section c, to derive $z(T)$. Appendix B, section d, derives the profiles of saturation vapor pressure and total pressure. The analytical equations are then summarized in appendix B, section e.

a. Derivation of Γ

The first half of this derivation follows R14. To begin, we note that the saturation specific humidity q_v^* is related to the saturation vapor pressure p_v^* by

$$q_v^* = \frac{R_a p_v^*}{R_v p}, \quad (\text{B1})$$

where R_a is the specific gas constant of dry air, R_v is the specific gas constant of water vapor, and p is the total air pressure. Here and elsewhere, we assume that the specific gas constant of moist air is well approximated by R_a . Next, we note that the Clausius–Clapeyron relation and the equation of hydrostatic balance can be written as

$$\partial_z \log(p_v^*) = -\frac{L\Gamma}{R_v T^2} \quad \text{and} \quad (\text{B2})$$

$$\partial_z \log(p) = -\frac{g}{R_a T}, \quad (\text{B3})$$

where $\Gamma \equiv -\partial_z T$ is the temperature lapse rate and L is the latent heat of evaporation. For simplicity, and because it will not have a significant effect on the results, we approximate L as a constant (i.e., independent of temperature). Later, we will set L equal to the latent heat of evaporation at an appropriately chosen reference temperature T_0 . Also, the ice phase and the associated latent heat of fusion are ignored here. Since the latent heat of fusion is only about 10% as large as the latent heat of evaporation, its omission does not have a significant effect on the results.

By taking the logarithm of Eq. (B1), differentiating with respect to height, and using Eqs. (B2) and (B3), we find that q_v^* obeys

$$\partial_z \log(q_v^*) = -\gamma, \quad (\text{B4})$$

where

$$\gamma = \frac{L\Gamma}{R_v T^2} - \frac{g}{R_a T}. \quad (\text{B5})$$

We may refer to γ as the fractional water vapor lapse rate. Note that $1/\gamma$ is the scale height for q_v^* .

Ignoring the small virtual effects of water vapor and condensates, the zero-buoyancy approximation requires that the clouds and the environment have the same temperature at each height. As described in R14, this reduces the bulk-plume equations for water vapor to

$$\partial_z q_v^* = \varepsilon(q_v - q_v^*) - c/M \quad \text{and} \quad (\text{B6})$$

$$-\partial_z q_v = \delta(q_v^* - q_v) + \alpha c/M, \quad (\text{B7})$$

where q_v^* is the specific humidity within the saturated updrafts (unitless, since q_v^* is a mass fraction), q_v is the specific humidity within the subsaturated environment, M is the convective mass flux ($\text{kg m}^{-2} \text{s}^{-1}$), ε is the fractional entrainment rate (m^{-1}), δ is the fractional detrainment rate (m^{-1}), c is the condensation rate within updrafts ($\text{kg m}^{-3} \text{s}^{-1}$), and α is the ratio of condensate evaporation in the environment to the water vapor condensation in the updrafts. Using the C and E notation adopted in section 1, the gross condensational heating is $C = Lc$, and the gross evaporative cooling is $E = \alpha Lc$. Therefore, the precipitation efficiency (PE) is equal to $(C - E)/C = 1 - \alpha$.

Writing q_v as $q_v = \text{RH}q_v^*$ and assuming that the fractional variations in RH are small over a distance $1/\gamma$, we can approximate these equations as

$$-\gamma q_v^* = \varepsilon(\text{RH} - 1)q_v^* - c/M \quad \text{and} \quad (\text{B8})$$

$$\text{RH} \gamma q_v^* = \delta(1 - \text{RH})q_v^* + \alpha c/M. \quad (\text{B9})$$

These two equations can be solved for RH and c/M , giving

$$\text{RH} = \frac{\delta + \alpha\gamma - \alpha\varepsilon}{\delta + \gamma - \alpha\varepsilon} \quad \text{and} \quad (\text{B10})$$

$$\frac{c}{M} = \frac{\delta + \gamma - \varepsilon}{\delta + \gamma - \alpha\varepsilon} \gamma q_v^*. \quad (\text{B11})$$

Equation (B10) is identical to Eq. (24) of R14.

As in R14, our next step is to write down two equations for the moist static energy (MSE) of updrafts that can be combined to give an expression for Γ . The MSE for the unsaturated environment is $h = c_p T + gz + Lq_v$, where we approximate c_p here as the heat capacity at constant pressure for dry air. Likewise, the MSE for a saturated cloud is $h^* = c_p T + gz + Lq_v^*$. Using Eq. (B4), we can write

$$\partial_z h^* = -c_p \Gamma + g - L\gamma q_v^*.$$

Using Eq. (B2), we can write this as

$$\partial_z h^* = g \left(1 + \frac{q_v^* L}{R_a T} \right) - \Gamma \left(c_p + \frac{q_v^* L^2}{R_v T^2} \right). \quad (\text{B12})$$

The second equation for h^* is obtained by writing down the bulk-plume equation for the updraft MSE:

$$\begin{aligned} \partial_z h^* &= \varepsilon(h - h^*) \\ &= \varepsilon L(q_v - q_v^*) \\ &= \varepsilon(\text{RH} - 1)Lq_v^*. \end{aligned} \quad (\text{B13})$$

We now depart from the derivation of R14 by assuming that M , RH, and α are all constant with height. The constancy of M with height requires that $\varepsilon = \delta$. Using the assumption of constant α , Eq. (B10) then implies that ε is proportional to γ . Let us define the constant a as $a = (1 - \alpha)\varepsilon/\gamma$. The entrainment rate, detrainment rate, the relative humidity from Eq. (B10), and the condensation rate from Eq. (B11) can then be written as

$$\varepsilon = \delta = \frac{a\gamma}{1 - \alpha}, \quad (\text{B14})$$

$$\text{RH} = \frac{\alpha + a}{1 + a}, \quad \text{and} \quad (\text{B15})$$

$$\frac{c}{M} = \frac{\gamma q_v^*}{1 + a}. \quad (\text{B16})$$

Substituting Eqs. (B14) and (B15) into Eq. (B13), we get

$$\partial_z h^* = -\frac{a}{a + 1} \gamma L q_v^*. \quad (\text{B17})$$

Note that $\gamma L q_v^* = -L \partial_z q_v^*$, so this can be written as $\partial_z h_a^* = 0$, where

$$h_a^* = c_p T + gz + \frac{Lq_v^*}{1+a} \quad (\text{B18})$$

is a conserved variable for the entraining clouds, which we refer to as the entraining moist static energy.

Finally, equating the right-hand sides of Eqs. (B12) and (B17) and using Eq. (B5) to express γ in terms of Γ , we can solve for Γ to find

$$\Gamma = \frac{(1+a)g + (q_v^* L g / R_a T)}{(1+a)c_p + (q_v^* L^2 / R_v T^2)}. \quad (\text{B19})$$

b. Derivation of $q_v^*(T)$

We can describe the vertical profile of q_v^* as a function of temperature by dividing Eq. (B4) by Γ and using the definition of γ from Eq. (B5), which gives

$$\frac{d}{dT} \log(q_v^*) = \frac{L}{R_v T^2} - \frac{g}{R_a \Gamma T}.$$

Using Eq. (B19) to eliminate Γ , this becomes

$$\frac{d}{dT} \log(q_v^*) = \frac{(R_a L / R_v T) - c_p}{R_a T + [q_v^* L / (1+a)]}.$$

To facilitate an analytical solution, we will approximate the two explicit temperatures on the right-hand side by a constant temperature T_0 . The equation can then be rearranged as

$$\left(\frac{R_a T_0}{q_v^*} + \frac{L}{1+a} \right) dq_v^* = \left(\frac{R_a L}{R_v T_0} - c_p \right) dT. \quad (\text{B20})$$

Denoting the surface temperature by T_s , we now integrate this equation from T to T_s to obtain

$$\log\left(\frac{q_{vs}^*}{q_v^*}\right) + \frac{L}{(1+a)R_a T_0} (q_{vs}^* - q_v^*) = f(T_s - T),$$

where q_{vs}^* is the saturation specific humidity at the surface, the constant T_0 is chosen to be $(T_s + T_{\text{FAT}})/2$ to be as representative as possible of the temperature experienced between T_s and T_{FAT} , and

$$f = \frac{L}{R_v T_0^2} - \frac{c_p}{R_a T_0}. \quad (\text{B21})$$

Exponentiating and rearranging, we obtain

$$\frac{Lq_v^*}{(1+a)R_a T_0} \exp\left[\frac{Lq_v^*}{(1+a)R_a T_0}\right] = y_a e^{-f(T_s - T)}, \quad (\text{B22})$$

where

$$y_a = \frac{Lq_{vs}^*}{(1+a)R_a T_0} \exp\left[\frac{Lq_{vs}^*}{(1+a)R_a T_0}\right]. \quad (\text{B23})$$

Taking the Lambert W function of both sides of Eq. (B22), and noting that the Lambert W function is defined by $W(xe^x) = x$, we get

$$q_v^*(T) = (1+a) \frac{R_a T_0}{L} W[y_a e^{-f(T_s - T)}]. \quad (\text{B24})$$

c. Derivation of $z(T)$

To obtain $z(T)$, we first rearrange Eq. (B19) for Γ as

$$\frac{(1+a)c_p + (q_v^* L^2 / R_v T^2)}{(1+a)g + (q_v^* L g / R_a T)} dT = -dz.$$

Replacing the explicit instances of T with T_0 and using Eq. (B24) to replace q_v^* , this can then be integrated to give

$$z(T) = z_s + \frac{c_p}{g} (T_s - T) + \frac{R_a T_0}{g} W[y_a e^{-f(T_s - T)}], \quad (\text{B25})$$

where z_s is the height of the surface, T_0 is once again chosen to be $(T_s + T_{\text{FAT}})/2$, and y_a and f are as defined in Eqs. (B23) and (B21).

d. Derivation of p_v^* and p

In the derivations of $q_v^*(T)$ and $z(T)$, we have approximated some of the instances of T by T_0 . To be consistent with these approximations when we derive $p_v^*(T)$ and $p(T)$, we must approximate the explicit instances of T as T_0 on the right-hand sides of Eqs. (B2) and (B3). Those equations can then be integrated to give

$$p_v^*(T) = p_{vs}^* \exp\left[\frac{L}{R_v T_0^2} (T - T_s)\right] \quad \text{and} \quad (\text{B26})$$

$$p(T) = p_s \exp\left\{\frac{-g[z(T) - z_s]}{R_a T_0}\right\}, \quad (\text{B27})$$

where p_{vs}^* is the water vapor saturation pressure at the surface, p_s is the total surface pressure, and $z(T)$ is given by Eq. (B25). It is straightforward to check that the expression for specific humidity produced by combining Eqs. (B1), (B26), and (B27) is identical to Eq. (B24).

e. Summary of equations

In summary, we have obtained an analytical solution to radiative-convective equilibrium in the case of height-invariant mass flux, relative humidity, and precipitation efficiency:

$$\begin{aligned} z(T) &= z_s + \frac{c_p}{g}(T_s - T) + \frac{R_a T_0}{g} W(y_a) \\ &\quad - \frac{R_a T_0}{g} W[y_a e^{-f(T_s - T)}], \end{aligned} \quad (\text{B28})$$

$$p(T) = p_s \exp\left\{\frac{-g[z(T) - z_s]}{R_a T_0}\right\}, \quad (\text{B29})$$

$$p_v^*(T) = p_{vs}^* \exp\left[\frac{L}{R_v T_0^2}(T - T_s)\right], \quad (\text{B30})$$

$$q_v^*(T) = \frac{R_a p_v^*(T)}{R_v p(T)} = (1 + a) \frac{R_a T_0}{L} W[y_a e^{-f(T_s - T)}], \quad (\text{B31})$$

and

$$q_v(T) = \text{RH} q_v^*(T). \quad (\text{B32})$$

APPENDIX C

Derivation of Eq. (27)

Here, we derive Eq. (27), which gives an approximate expression for upper-tropospheric Δh^* as a function of near-surface saturation water vapor mass fraction q_{vs}^* . To begin, note that the moist static energy (MSE) of the undiluted parcel can be written as either

$$h^*(z) = c_p T_u(z) + gz + Lq_{vu}^*(z),$$

where the subscript u is used to remind us that these are the temperature and water mass fraction of the *undiluted* parcel, or as

$$h^*(z_s) = c_p T_s + gz_s + Lq_{vs}^*.$$

Since MSE is conserved for the undiluted parcel,

$$h^*(z) = h^*(z_s). \quad (\text{C1})$$

The saturated EMSE of the environment (also, the EMSE of the diluted parcel) can be written as either

$$h_a^*(z) = c_p T(z) + gz + \frac{Lq_v^*(z)}{1 + a}$$

or as

$$h_a^*(z_s) = c_p T_s + gz_s + \frac{Lq_{vs}^*}{1 + a}.$$

Since saturated entraining moist static energy is constant with height for the environment,

$$h_a^*(z) = h_a^*(z_s). \quad (\text{C2})$$

Subtracting Eq. (C2) from Eq. (C1), we get $h^*(z) - h_a^*(z) = h^*(z_s) - h_a^*(z_s)$, which can be written as

$$\begin{aligned} &[c_p T_u(z) + gz + Lq_{vu}^*(z)] - \left[c_p T(z) + gz + \frac{Lq_v^*(z)}{1 + a}\right] \\ &= (c_p T_s + gz_s + Lq_{vs}^*) - \left(c_p T_s + gz_s + \frac{Lq_{vs}^*}{1 + a}\right). \end{aligned}$$

This can be rearranged to give

$$\begin{aligned} &[c_p T_u(z) + gz + Lq_{vu}^*(z)] - [c_p T(z) + gz + Lq_v^*(z)] \\ &= \frac{a}{1 + a} L[q_{vs}^* - q_v^*(z)]. \end{aligned}$$

Noting that the left-hand side is the difference in saturated MSE (not saturated EMSE) between the undiluted parcel and the environment, we obtain

$$\Delta h^*(z) = \frac{a}{1 + a} L[q_{vs}^* - q_v^*(z)]. \quad (\text{C3})$$

This says that, at height z , the difference in MSE between the undiluted parcel and the environment Δh is proportional to the difference in saturated water vapor mass fraction between the surface and height z . For all but the largest T_s , q_v^* at the tropopause is sufficiently small that it can be safely dropped from this equation, so we arrive at Eq. (27).

REFERENCES

- Brewer, A. W., 1949: Evidence for a world circulation provided by the measurements of helium and water vapour distribution in the stratosphere. *Quart. J. Roy. Meteor. Soc.*, **75**, 351–363, doi:[10.1002/qj.49707532603](https://doi.org/10.1002/qj.49707532603).
- Brooks, H. E., C. A. Doswell III, and J. Cooper, 1994: On the environments of tornadic and nontornadic mesocyclones. *Wea. Forecasting*, **9**, 606–618, doi:[10.1175/1520-0434\(1994\)009<0606:OTEOTA>2.0.CO;2](https://doi.org/10.1175/1520-0434(1994)009<0606:OTEOTA>2.0.CO;2).
- , J. W. Lee, and J. P. Craven, 2003: The spatial distribution of severe thunderstorm and tornado environments from global reanalysis data. *Atmos. Res.*, **67–68**, 73–94, doi:[10.1016/S0169-8095\(03\)00045-0](https://doi.org/10.1016/S0169-8095(03)00045-0).
- Diffenbaugh, N. S., M. Scherer, and R. J. Trapp, 2013: Robust increases in severe thunderstorm environments in response to greenhouse forcing. *Proc. Natl. Acad. Sci. USA*, **110**, 16 361–16 366, doi:[10.1073/pnas.1307758110](https://doi.org/10.1073/pnas.1307758110).
- Emanuel, K. A., and M. Bister, 1996: Moist convective velocity and buoyancy scales. *J. Atmos. Sci.*, **53**, 3276–3285, doi:[10.1175/1520-0469\(1996\)053<3276:MCVABS>2.0.CO;2](https://doi.org/10.1175/1520-0469(1996)053<3276:MCVABS>2.0.CO;2).
- Ferrier, B. S., J. Simpson, and W.-K. Tao, 1996: Factors responsible for precipitation efficiencies in midlatitude and tropical squall simulations. *Mon. Wea. Rev.*, **124**, 2100–2125, doi:[10.1175/1520-0493\(1996\)124<2100:FRFPEI>2.0.CO;2](https://doi.org/10.1175/1520-0493(1996)124<2100:FRFPEI>2.0.CO;2).
- Fierro, A. O., J. M. Simpson, M. A. Lemone, J. M. Straka, and B. F. Smull, 2009: On how hot towers fuel the Hadley cell: An observational and modeling study of line-organized convection in the equatorial trough from TOGA COARE. *J. Atmos. Sci.*, **66**, 2730–2746, doi:[10.1175/2009JAS3017.1](https://doi.org/10.1175/2009JAS3017.1).
- Harrop, B. E., and D. L. Hartmann, 2012: Testing the role of radiation in determining tropical cloud-top temperature. *J. Climate*, **25**, 5731–5747, doi:[10.1175/JCLI-D-11-00445.1](https://doi.org/10.1175/JCLI-D-11-00445.1).

- Hartmann, D., and K. Larson, 2002: An important constraint on tropical cloud–climate feedback. *Geophys. Res. Lett.*, **29**, 1951, doi:[10.1029/2002GL015835](https://doi.org/10.1029/2002GL015835).
- Johns, R., and C. Doswell III, 1992: Severe local storms forecasting. *Wea. Forecasting*, **7**, 588–612, doi:[10.1175/1520-0434\(1992\)007<0588:SLSF>2.0.CO;2](https://doi.org/10.1175/1520-0434(1992)007<0588:SLSF>2.0.CO;2).
- Kuang, Z., and C. S. Bretherton, 2006: A mass-flux scheme view of a high-resolution simulation of a transition from shallow to deep cumulus convection. *J. Atmos. Sci.*, **63**, 1895–1909, doi:[10.1175/JAS3723.1](https://doi.org/10.1175/JAS3723.1).
- , and D. Hartmann, 2007: Testing the fixed anvil temperature hypothesis in a cloud-resolving model. *J. Climate*, **20**, 2051–2057, doi:[10.1175/JCLI4124.1](https://doi.org/10.1175/JCLI4124.1).
- Langhans, W., K. Yeo, and D. M. Romps, 2015: Lagrangian investigation of the precipitation efficiency of convective clouds. *J. Atmos. Sci.*, **72**, 1045–1062, doi:[10.1175/JAS-D-14-0159.1](https://doi.org/10.1175/JAS-D-14-0159.1).
- Lipps, F. B., and R. S. Hemler, 1986: Numerical simulation of deep tropical convection associated with large-scale convergence. *J. Atmos. Sci.*, **43**, 1796–1816, doi:[10.1175/1520-0469\(1986\)043<1796:NSODTC>2.0.CO;2](https://doi.org/10.1175/1520-0469(1986)043<1796:NSODTC>2.0.CO;2).
- Mapes, B. E., 2001: Water's two height scales: The moist adiabat and the radiative troposphere. *Quart. J. Roy. Meteor. Soc.*, **127**, 2353–2366, doi:[10.1002/qj.49712757708](https://doi.org/10.1002/qj.49712757708).
- Muller, C. J., P. A. O'Gorman, and L. E. Back, 2011: Intensification of precipitation extremes with warming in a cloud-resolving model. *J. Climate*, **24**, 2784–2800, doi:[10.1175/2011JCLI3876.1](https://doi.org/10.1175/2011JCLI3876.1).
- Murugavel, P., S. D. Pawar, and V. Gopalakrishnan, 2014: Climatology of lightning over Indian region and its relationship with convective available potential energy. *Int. J. Climatol.*, **34**, 3179–3187, doi:[10.1002/joc.3901](https://doi.org/10.1002/joc.3901).
- Pauluis, O., and I. M. Held, 2002a: Entropy budget of an atmosphere in radiative–convective equilibrium. Part I: Maximum work and frictional dissipation. *J. Atmos. Sci.*, **59**, 125–139, doi:[10.1175/1520-0469\(2002\)059<0125:EBOAAI>2.0.CO;2](https://doi.org/10.1175/1520-0469(2002)059<0125:EBOAAI>2.0.CO;2).
- , and —, 2002b: Entropy budget of an atmosphere in radiative–convective equilibrium. Part II: Latent heat transport and moist processes. *J. Atmos. Sci.*, **59**, 140–149, doi:[10.1175/1520-0469\(2002\)059<0140:EBOAAI>2.0.CO;2](https://doi.org/10.1175/1520-0469(2002)059<0140:EBOAAI>2.0.CO;2).
- , V. Balaji, and I. Held, 2000: Frictional dissipation in a precipitating atmosphere. *J. Atmos. Sci.*, **57**, 989–994, doi:[10.1175/1520-0469\(2000\)057<0989:FDIAPA>2.0.CO;2](https://doi.org/10.1175/1520-0469(2000)057<0989:FDIAPA>2.0.CO;2).
- Pawar, S. D., D. M. Lal, and P. Murugavel, 2012: Lightning characteristics over central India during Indian summer monsoon. *Atmos. Res.*, **106**, 44–49, doi:[10.1016/j.atmosres.2011.11.007](https://doi.org/10.1016/j.atmosres.2011.11.007).
- Rasmussen, E. N., 2003: Refined supercell and tornado forecast parameters. *Wea. Forecasting*, **18**, 530–535, doi:[10.1175/1520-0434\(2003\)18<530:RSATFP>2.0.CO;2](https://doi.org/10.1175/1520-0434(2003)18<530:RSATFP>2.0.CO;2).
- , and D. O. Blanchard, 1998: A baseline climatology of sounding-derived supercell and tornado forecast parameters. *Wea. Forecasting*, **13**, 1148–1164, doi:[10.1175/1520-0434\(1998\)013<1148:ABCOSD>2.0.CO;2](https://doi.org/10.1175/1520-0434(1998)013<1148:ABCOSD>2.0.CO;2).
- Rennó, N. O., and A. P. Ingersoll, 1996: Natural convection as a heat engine: A theory for CAPE. *J. Atmos. Sci.*, **53**, 572–585, doi:[10.1175/1520-0469\(1996\)053<0572:NCAHE>2.0.CO;2](https://doi.org/10.1175/1520-0469(1996)053<0572:NCAHE>2.0.CO;2).
- Romps, D. M., 2008: The dry-entropy budget of a moist atmosphere. *J. Atmos. Sci.*, **65**, 3779–3799, doi:[10.1175/2008JAS2679.1](https://doi.org/10.1175/2008JAS2679.1).
- , 2010: A direct measure of entrainment. *J. Atmos. Sci.*, **67**, 1908–1927, doi:[10.1175/2010JAS3371.1](https://doi.org/10.1175/2010JAS3371.1).
- , 2011: Response of tropical precipitation to global warming. *J. Atmos. Sci.*, **68**, 123–138, doi:[10.1175/2010JAS3542.1](https://doi.org/10.1175/2010JAS3542.1).
- , 2014a: An analytical model for tropical relative humidity. *J. Climate*, **27**, 7432–7449, doi:[10.1175/JCLI-D-14-00255.1](https://doi.org/10.1175/JCLI-D-14-00255.1).
- , 2014b: Rayleigh damping in the free troposphere. *J. Atmos. Sci.*, **71**, 553–565, doi:[10.1175/JAS-D-13-062.1](https://doi.org/10.1175/JAS-D-13-062.1).
- , 2015: MSE minus CAPE is the true conserved variable for an adiabatically lifted parcel. *J. Atmos. Sci.*, **72**, 3639–3646, doi:[10.1175/JAS-D-15-0054.1](https://doi.org/10.1175/JAS-D-15-0054.1).
- , and Z. Kuang, 2010: Do undiluted convective plumes exist in the upper tropical troposphere? *J. Atmos. Sci.*, **67**, 468–484, doi:[10.1175/2009JAS3184.1](https://doi.org/10.1175/2009JAS3184.1).
- , and R. Öktem, 2015: Stereo photogrammetry reveals substantial drag on cloud thermals. *Geophys. Res. Lett.*, **42**, 5051–5057, doi:[10.1002/2015GL064009](https://doi.org/10.1002/2015GL064009).
- , J. T. Seeley, D. Vollaro, and J. Molinari, 2014: Projected increase in lightning strikes in the United States due to global warming. *Science*, **346**, 851–854, doi:[10.1126/science.1259100](https://doi.org/10.1126/science.1259100).
- Seeley, J. T., and D. M. Romps, 2015a: The effect of global warming on severe thunderstorms in the United States. *J. Climate*, **28**, 2443–2458, doi:[10.1175/JCLI-D-14-00382.1](https://doi.org/10.1175/JCLI-D-14-00382.1).
- , and —, 2015b: Why does tropical convective available potential energy (CAPE) increase with warming? *Geophys. Res. Lett.*, **42**, 10429–10437, doi:[10.1002/2015GL066199](https://doi.org/10.1002/2015GL066199).
- , and —, 2016: Tropical cloud buoyancy is the same in a world with or without ice. *Geophys. Res. Lett.*, **43**, 3572–3579, doi:[10.1002/2016GL068583](https://doi.org/10.1002/2016GL068583).
- Singh, M. S., and P. A. O'Gorman, 2013: Influence of entrainment on the thermal stratification in simulations of radiative-convective equilibrium. *Geophys. Res. Lett.*, **40**, 4398–4403, doi:[10.1002/grl.50796](https://doi.org/10.1002/grl.50796).
- , and —, 2015: Increases in moist-convective updraft velocities with warming in radiative-convective equilibrium. *Quart. J. Roy. Meteor. Soc.*, **141**, 2828–2838, doi:[10.1002/qj.2567](https://doi.org/10.1002/qj.2567).
- Sobel, A. H., and S. J. Camargo, 2011: Projected future seasonal changes in tropical summer climate. *J. Climate*, **24**, 473–487, doi:[10.1175/2010JCLI3748.1](https://doi.org/10.1175/2010JCLI3748.1).
- Tao, W. K., D. Johnson, C. L. Shie, and J. Simpson, 2004: The atmospheric energy budget and large-scale precipitation efficiency of convective systems during TOGA COARE, GATE, SCSMEX, and ARM: Cloud-resolving model simulations. *J. Atmos. Sci.*, **61**, 2405–2423, doi:[10.1175/1520-0469\(2004\)061<2405:TAEBAL>2.0.CO;2](https://doi.org/10.1175/1520-0469(2004)061<2405:TAEBAL>2.0.CO;2).
- Trapp, R. J., N. S. Diffenbaugh, H. E. Brooks, M. E. Baldwin, E. D. Robinson, and J. S. Pal, 2007: Changes in severe thunderstorm environment frequency during the 21st century caused by anthropogenically enhanced global radiative forcing. *Proc. Natl. Acad. Sci. USA*, **104**, 19 719–19 723, doi:[10.1073/pnas.0705494104](https://doi.org/10.1073/pnas.0705494104).
- , —, and A. Gluhovsky, 2009: Transient response of severe thunderstorm forcing to elevated greenhouse gas concentrations. *Geophys. Res. Lett.*, **36**, L01703, doi:[10.1029/2008GL036203](https://doi.org/10.1029/2008GL036203).
- Weisman, M. L., and J. B. Klemp, 1982: The dependence of numerically simulated convective storms on vertical wind shear and buoyancy. *Mon. Wea. Rev.*, **110**, 504–520, doi:[10.1175/1520-0493\(1982\)110<0504:TDONSC>2.0.CO;2](https://doi.org/10.1175/1520-0493(1982)110<0504:TDONSC>2.0.CO;2).
- Williams, E., and N. Renno, 1993: An analysis of the conditional instability of the tropical atmosphere. *Mon. Wea. Rev.*, **121**, 21–36, doi:[10.1175/1520-0493\(1993\)121<0021:AAOTCI>2.0.CO;2](https://doi.org/10.1175/1520-0493(1993)121<0021:AAOTCI>2.0.CO;2).
- , S. G. Geotis, N. Renno, S. A. Rutledge, E. Rasmussen, and T. Rickenbach, 1992: A radar and electrical study of tropical “hot towers.” *J. Atmos. Sci.*, **49**, 1386–1395, doi:[10.1175/1520-0469\(1992\)049<1386:ARAESO>2.0.CO;2](https://doi.org/10.1175/1520-0469(1992)049<1386:ARAESO>2.0.CO;2).
- , and Coauthors, 2002: Contrasting convective regimes over the Amazon: Implications for cloud electrification. *J. Geophys. Res.*, **107**, 8082, doi:[10.1029/2001JD000380](https://doi.org/10.1029/2001JD000380).
- Zelinka, M. D., and D. L. Hartmann, 2010: Why is longwave cloud feedback positive? *J. Geophys. Res.*, **115**, D16117, doi:[10.1029/2010JD013817](https://doi.org/10.1029/2010JD013817).